(2)

HACT SPATIAL LIGHT MODULATOR

Contract N00014-91-C-0090

April 1, 1991 - April 30, 1992

Final Report R92-970069-F

To

Office of Naval Research

By

...dkowski - UTRC Prime Contract
F.C. Jain - UConn - Subcontract

DISCLAIMER NOTICE

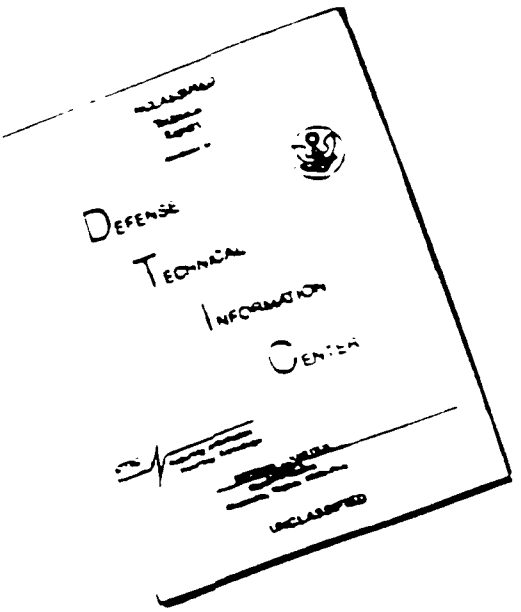

THIS DOCUMENT IS BEST QUALITY AVAILABLE. THE COPY FURNISHED TO DTIC CONTAINED A SIGNIFICANT NUMBER OF PAGES WHICH DO NOT REPRODUCE LEGIBLY.

REPORT DOCUMENTATION PAGE

Form Approved
OMB No. 0704-0188

1. AGENCY USE ONLY (Leave blank)	2. REPORT DATE	3. REPORT TYPE AND DATES COVERED
	9/92	Final 4-1-91 - 4-30-92

4. TITLE AND SUBTITLE
HACT SPATIAL LIGHT MODULATOR

5. FUNDING NUMBERS
N00014-91-C-0090

6. AUTHOR(S)
Thomas W. Grudkowski
Faquir C. Jain

7. PERFORMING ORGANIZATION NAME(S) AND ADDRESS(ES)
United Technologies Corporation
United Technologies Research Center
400 Main Street
East Hartford, Connecticut 06108

8. PERFORMING ORGANIZATION REPORT NUMBER
R92-970069-F

9. SPONSORING/MONITORING AGENCY NAME(S) AND ADDRESS(ES)
Office of Naval Research ATTN: William Miceli
Department of Navy
800 N. Quincy Street
Arlington, VA 22217-5000

10. SPONSORING/MONITORING AGENCY REPORT NUMBER

11. SUPPLEMENTARY NOTES
Subcontractor - University of Connecticut

12a. DISTRIBUTION/AVAILABILITY STATEMENT
DISTRIBUTION STATEMENT A
Approved for public release;
Distribution Unlimited

12b. DISTRIBUTION CODE

13. ABSTRACT (Maximum 200 words)

High contrast ratio exceeding 1200:1 has been obtained in Fabry-Perot structures consisting of InGaAs-GaAs multiple quantum well layers and AlAs/GaAs dielectric mirrors on GaAs substrates. The tuning voltage ranges between 5-25 volts, and the wavelength shifts between 4-10 nm. The on-loss is about 5dB. The design of coupled-cavity Fabry-Perot structures have been completed to obtain a contrast of over 6000:1, and the fabrication is in progress. These structures are designed to yield lower on-loss along with a wider transmission spectrum of 1nm.

Heterojunction Acoustic Charge Transport (HACT) devices have been fabricated in various formats including freeze frame feature. The HACT device is a type of CCD which uses a surface acoustic wave to propagate charge along an AlGaAs/GaAs heterostructure. It provides a method of addressing the SLM array without using multiple interconnect circuits. The integration of HACT with MQW SLM is in progress. This will be followed by the integration of Fabry-Perot structures with HACT system to obtain high contrast SLMs. Design of these structures has been completed, and fabrication has been initiated. Single-channel HACT-SLMs, consisting of up to 1000 pixels, will be developed in the next two years. 2-D SLM devices having power consumption of 1 Watt per 100,000 pixels are possible.

14. SUBJECT TERMS	15. NUMBER OF PAGES
Spatial Light Modulator, Optical Computing, Heterojunction Acoustic Charge Transport Device, Gallium Arsenide, Multiple Quantum Well, Stark Effect	90
	16. PRICE CODE

17. SECURITY CLASSIFICATION OF REPORT	18. SECURITY CLASSIFICATION OF THIS PAGE	19. SECURITY CLASSIFICATION OF ABSTRACT	20. LIMITATION OF ABSTRACT
Unclassified	Unclassified	Unclassified	

Table of Contents

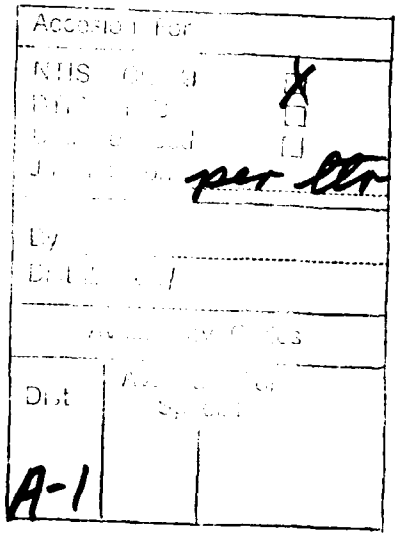

Heterojunction Acoustic Charge Transport (HACT) Spatial Light Modulators

T. Grudkowski, United Technologies Research Center
F. Jain, University of Connecticut

Summary

High contrast ratio exceeding 1200:1 has been obtained in Fabry-Perot structures consisting of InGaAs-GaAs multiple quantum well layers and AlAs.GaAs dielectric mirrors on GaAs substrates. The tuning voltage ranges between 5-25 volts, and the wavelength shifts between 4-10 nm. The on-loss is about 5 dB. The design of couples-cavity Fabry-Perot structures have been completed to obtain a contrast of over 6000:1, and the fabrication is in progress. These structures are designed to yield lower on-loss along with a wider transmission spectrum of > 1nm.

Heterojunction Acoustic Charge Transport (HACT) devices have been fabricated in various formats including freeze frame feature. The HACT device is a type of CCD which uses a surface acoustic wave to propagate charge laong an AlGaAs/GaAs heterostructure. It provides a method of addressing the SLM array without using multiple interconnect circuits. The integration of HACT with MQW SLM is in progress. This will be followed by the integration of Fabry-Perot structures with HACT system to obtain high contrast SLMs. Design of these structures has been completed, and fabrication has been initiated. Single-channel HACT-SLMs, consisting of up to 1000 pixels, will be developed in the next two years. 2-D SLM devices having power consumption of 1 Watt per 100,000 pixels are possible. The project summary chart is shown in Table A.

A. Project Description

A.0. Introduction

Multiple Quantum Well Modulators, employing shift of excitonic absorption and/or index of refraction in the presence of an externally applied/induced electric field, has drawn significant attention in the scientific community. In particular, two aspects of MQW modulators were stressed during the first year of the contract. These are the development of structures yielding high contrast ratios and method of two-dimensional addressing. A review paper by Jain, Bhattacharjee and Grudkowski [see appendix] is attached for background references.

Multifaceted progress was made during the first year of the contract:

1) Design and fabrication of Stark effect tunable high contrast Fabry-Perot modulators having AlAs- quarter wave Stack Mirror and InGaAs-GaAs Multiple Quantum Well Cavity (up to six microns of total growth by Molecular Beam Epitaxy).

2) Completion of Coupled-cavity design having over 1 nm bandwidth.

3) Design of Heterostructure Acoustic Charge Transport (HACT) Spatial Light Modulators (SLMs).

TABLE A

UNITED TECHNOLOGIES RESEARCH CENTER

Heterojunction Acoustic Charge Transport (HACT)

THE UNIVERSITY OF CONNECTICUT

MQW Spatial Light Modulator

Objectives:

- Demonstrate feasibility for achieving 10,000:1 contrast ratio in a HACT Multiple Quantum Well SLM, eventually in a 2-D structure.
- Achieve > 1 nm optical bandwidth

Approach:

- Apply quantum confined Stark effect (QCSE) to modulate light in multiple Quantum Well coupled-cavity structures to obtain a high contrast ratio
- Make use of Acoustic charge transport within HACT to achieve SLM operation
- Use high uniformity MBE growth techniques to fabricate the required III - V group semiconductor multi-layered structures

Status:

- Demonstrated Stark effect tunable contrast ratio of 1200:1 for a Fabry-Perot structure using InGaAs/GaAs MQW cavity.
- Fabricated Fabry-Perot cavity structure with nontunable contrast ratio greater than 6,000.
- Demonstrated (under UTRC/IRAD) charge freezing capability in HACT.
- Developed a high precision optical measurement system.
- Completed theoretical design of novel 10,000:1 contrast ratio HACT - SLM's.

Goals:

- 100 MHz modulation rate
- Contrast Ratio 10,000:1
- 10 μm x 10 μm pixel size

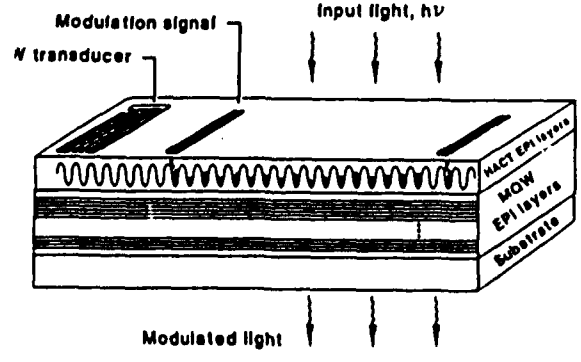

4) Modeling of Contrast ratio in Fabry-Perot modulators including: (a) wavefunctions in quantum wells, (b) Stark effect tuning , and (c) transmission through multilayered Fabry-Perot cavity structures.

5) Demonstration of charge freezing capability in HACT (UTRC/IRAD).

Detailed description of program achievements are given below.

A.1. Tunable Fabry-Perot Modulators using Quantum Confined Stark Effect (QCSE).

Tunable Fabry-Perot (F-P) modulators, consisting of strained InGaAs-GaAs MQW layers have been shown to yield a contrast over 1200:1. Tuning is achieved by varying the index of refraction of the MQW layers forming the cavity using quantum confined Stark effect. The mirrors are realized by AlAs-GaAs quarter wave $\lambda/4$ dielectric stacks having 12 and 15.5 periods respectively. The device has the potential of achieving even higher tunable contrast ratios when the period of the $\lambda/4$ mirrors are increased, ratios of 6000:1 have been achieved for a nontunable structure. Transmissivity and contrast ratios are presented for various wavelengths as a function of applied bias.

Optical modulators using Quantum Confined Stark effect (QCSE) have been reported by a number of investigators since the reporting of the QCSE by Miller et al. Recently, the emphasis has been to obtain high contrast ratios. Contrast ratios have been enhanced by manipulating the excitonic behavior of quantum wells, by utilizing coupled well MQW layers or by employing a high finesse Fabry-Perot cavity.

In the case of the Fabry-Perot cavity, the schemes include symmetrical mirrors (matched reflectivities), asymmetrical mirrors (different reflectivities for top and bottom mirrors) and saturable mirror structures. The use of a saturable back mirror, whose reflectivity can be controlled by an external pump (photoabsorbtive effect) has attracted significant attention. We have designed and fabricated symmetrical F-P modulators consisting of a single cavity F-P structure using InGaAs-GaAs MQW.

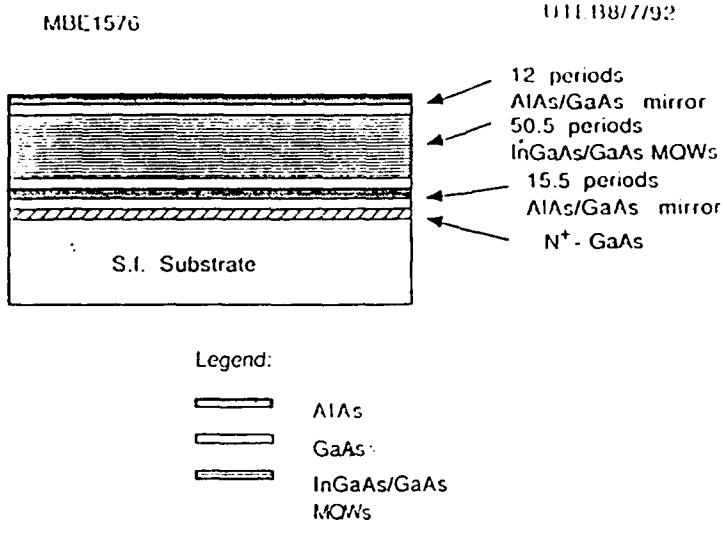

Figure 1

Figure 1 shows the schematic of a typical tunable F-P cavity optical modulator. It consists of a quarter wave stack of AlAs-GaAs dielectric mirrors (M1 and M2) enclosing an

InGaAs-GaAs MQW cavity. The thickness of AlAs and GaAs layers are 695 and 805Å, respectively, in the λ/4 stack layers. The InGaAs-GaAs MQW consists of 144 periods, with 50Å of InGaAs and 100A of GaAs making up one period, with a total thickness of about 2.0 μm.

The structure is grown using the molecular beam epitaxial system. AlAs-GaAs dielectric mirrors were implemented in place of AlGaAs-GaAs mirrors to obtain higher reflectivities. In addition, we believe that during the growth process, AlGaAs layers are more prone to variations than binary AlAs layers.

Fig. 2 shows a typical Stark effect tuning measurement in an InGaAs-GaAs MQW cavity. The contrasts are shown in the inset. The external voltage is applied across the *n*+ GaAs buffer layer and the top Schottky barrier contact. The buffer layer is contracted by etching a via and depositing a Au-Ge-Ni ohmic contact layer. In the case on n-GaAs substrate the contact can be made from the substrate side. It may be noted that in the present device, both mirrors (M1 and M2) are undoped. A combination of p and n dopings may be used for top and bottom mirrors to reduce the magnitude of the tuning voltage.

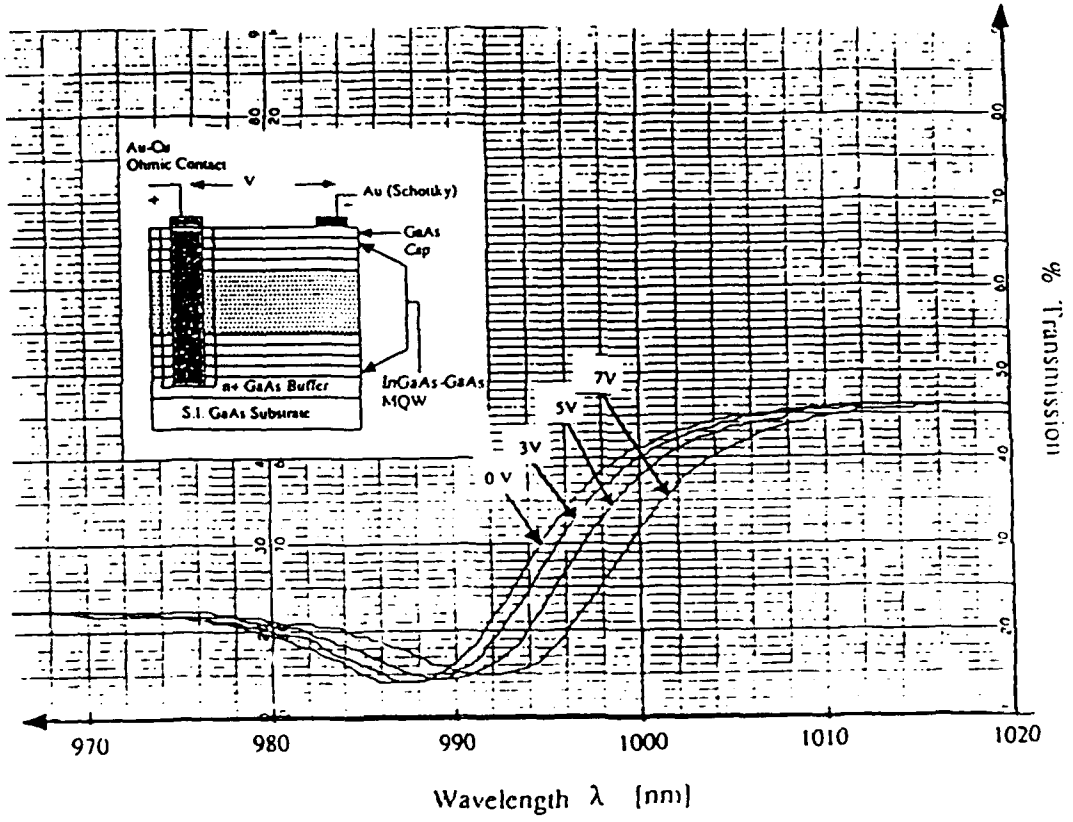

Figure 2

The measurement of Stark shifts in an InGaAs-GaAs MQW structure (as shown in the inset).

The measurement of transmitted intensity is shown in Figure 3. The tuning range is about 20 volts. The tuning wavelength is about 10nm. This is corroborated by results on InGaAs-GaAs modulators by several investigators.

Figure 4 summarizes the contrast ratio at various wavelength as a function of applied bias. This plot is computed from the data of Figure 3.

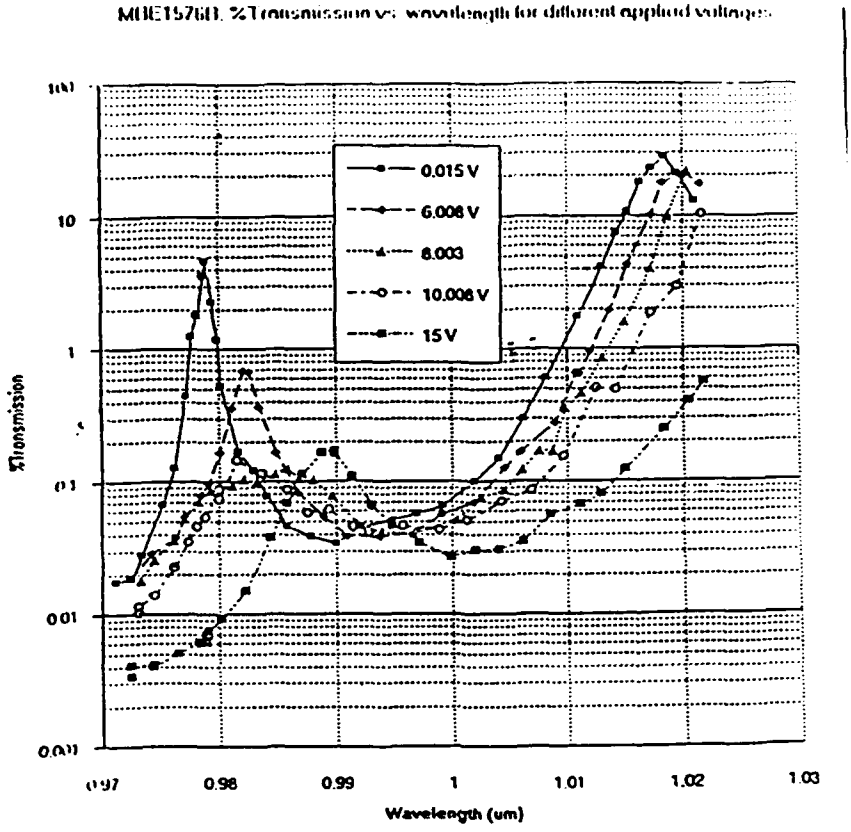

Figure 3

Transmission as a function of wavelength with applied bias as a parameter

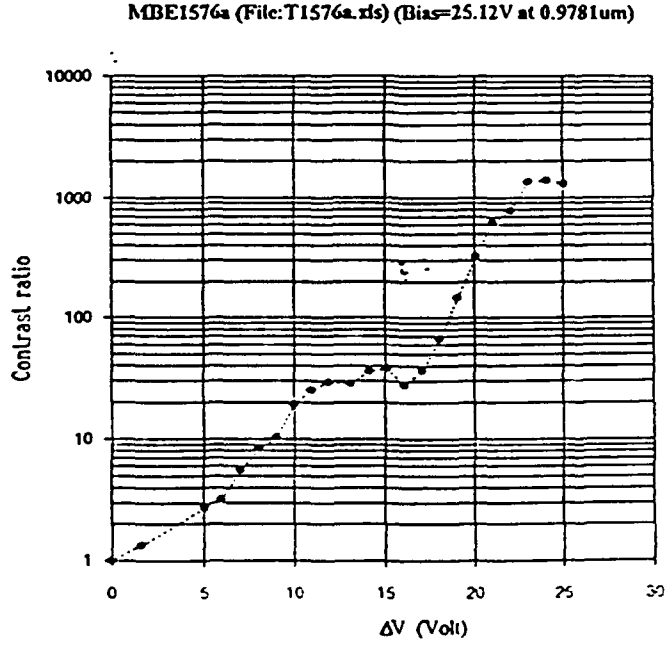

Figure 4

Variation of Contrast ratio with applied bias ΔV

The observed transmitted intensity of F-P is matched by simulations. The shift is corroborated by using in index charge of $\Delta n \approx 0.02$ in the InGaAs-GaAs Multiple Quantum Well layers forming the cavity. These computations are shown in Figure 5.

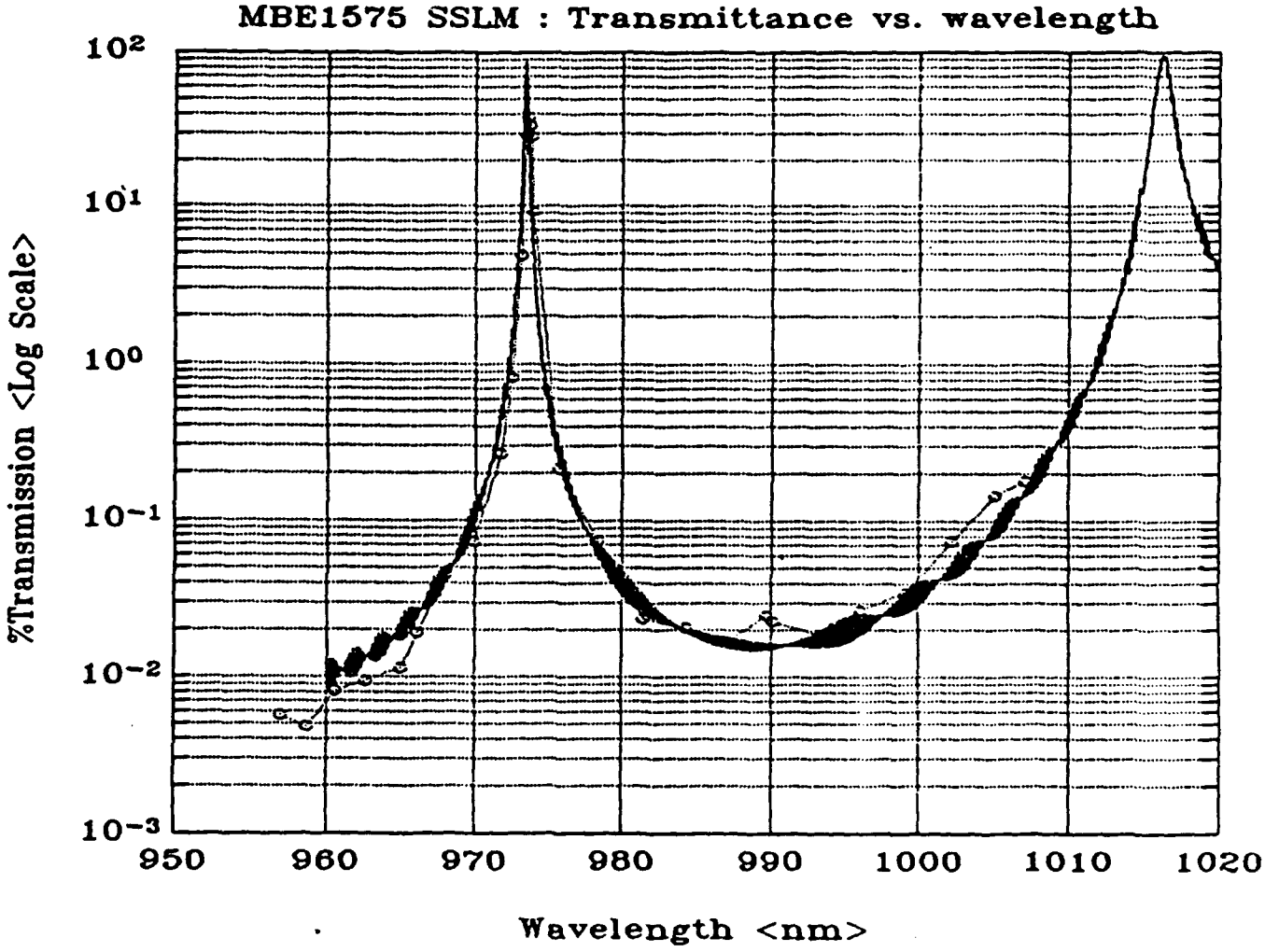

Figure 5

Experimental and Computed transmittance as a function of wavelength

A2. Coupled-Cavity Fabry-Perot Structure

High contrast ratios can be obtained in single Fabry-Perot Cavity Modulators. However, the increased contrast is associated with a narrow bandwidth. This not only requires careful tuning of the incident light (laser) source but also results in intensity loss of the peak. Coupled-cavity structures, such as shown in Figure 6, eliminate both of these problems. As can be seen from the simulations of transmitted intensity in Figure 7 the coupled-cavity structure yields a significantly higher bandwidth (2-3 nm)while maintaining a high contrast ratio. Experimental fabrication of these structures is in progress.

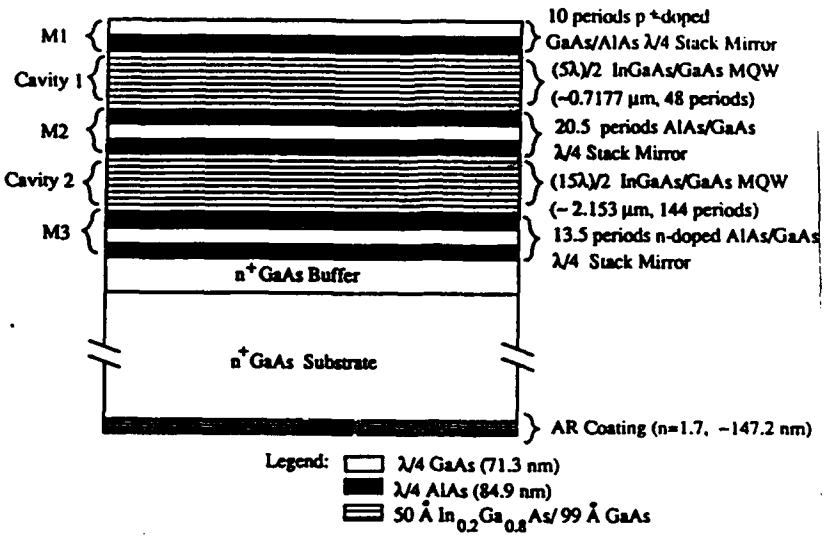

Figure 6

Asymmetric Coupled-Davity MQW SLM Structure
(Operating wavelength λ= 1,001 nm)

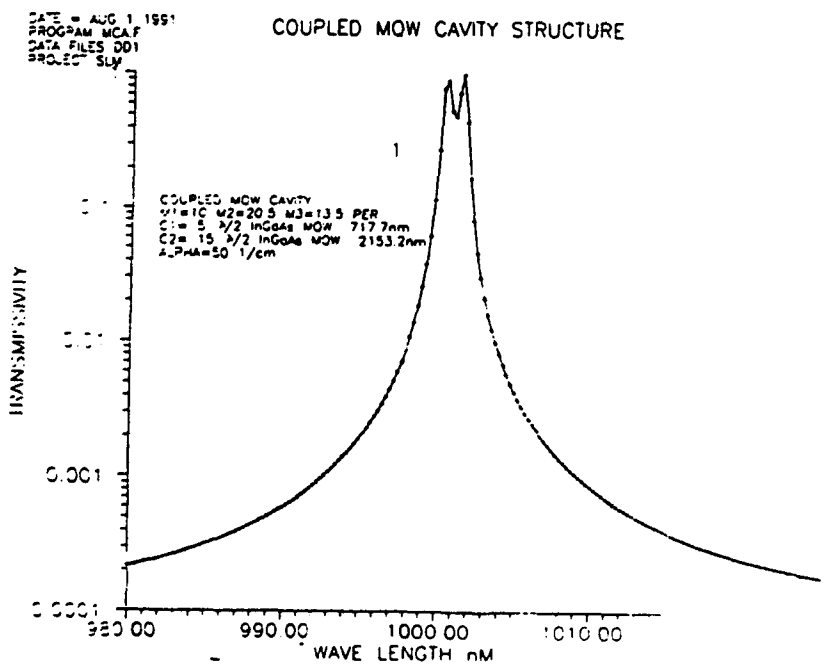

Figure 7

Transmission in a Coupled-Cavity Structure

A.3. Design of Heterostructure Acoustic Charge Transport (HACT) Spatial Light Modulators (SLMs)

Optical modulators can be addressed in a variety of ways. One of these approaches is to use charge-coupled devices (CCDs). Here, the magnitude of charge transported in the channel creates a corresponding electric field in the optical material, which in turn modulates the incident light. Kingston et al and Goodhue et al have used Franz-Keldysh effect (Figure 8) and Stark effect in multiple quantum wells (MQWs) Figure 9, respectively.

Our approach is to use the concept of heterostructure acoustic charge transport (HACT) which, unlike CCDs, requires no electrodes and associated clock circuits. Figure 10 describes a pixel using HACT based optical modulators. The presence of electron signal charge, which is transported in the NID GaAs well channel by a surface acoustic wave (SAW), induces an electric field in the undoped MQW layers (situated in proximity under the channel). The electric field in turn modulates the incident light via the quantum confined Stark effect (QCSE). A three-dimensional view of this device is shown in Figure 11.

HACT-SLMs, like other excitonic Stark effect based MQW devices, offers lower contrast ratios. Figures 12 and 13 show the schemes integrating Fabry-Perot cavities to enhance the contrast of HACT-SLMs. The simulation of transmitted intensity for a single F-P HACT-SLM (shown in Figure 13) is plotted in Figure 14. Note that HACT addressing system is on top of the Fabry-Perot cavity. This is in contrast to the structure of Figure 12.

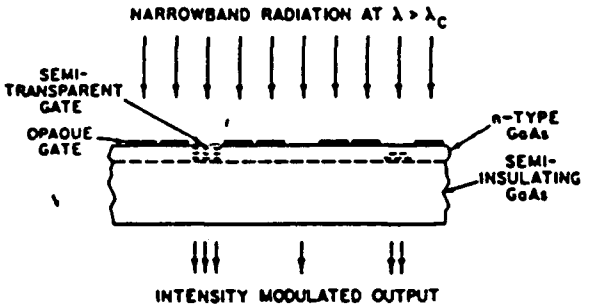

Figure 8

Schematic of spatial light modulator using a three-phase GaAs CCD
Kingston, et. al - Franz-Keldysh effect

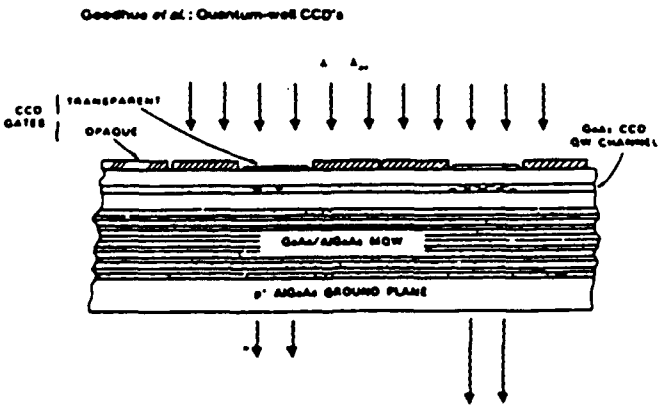

Figure 9

Goodhue, et al - QWCCD - Excitonic Absorption With E Field Dependence

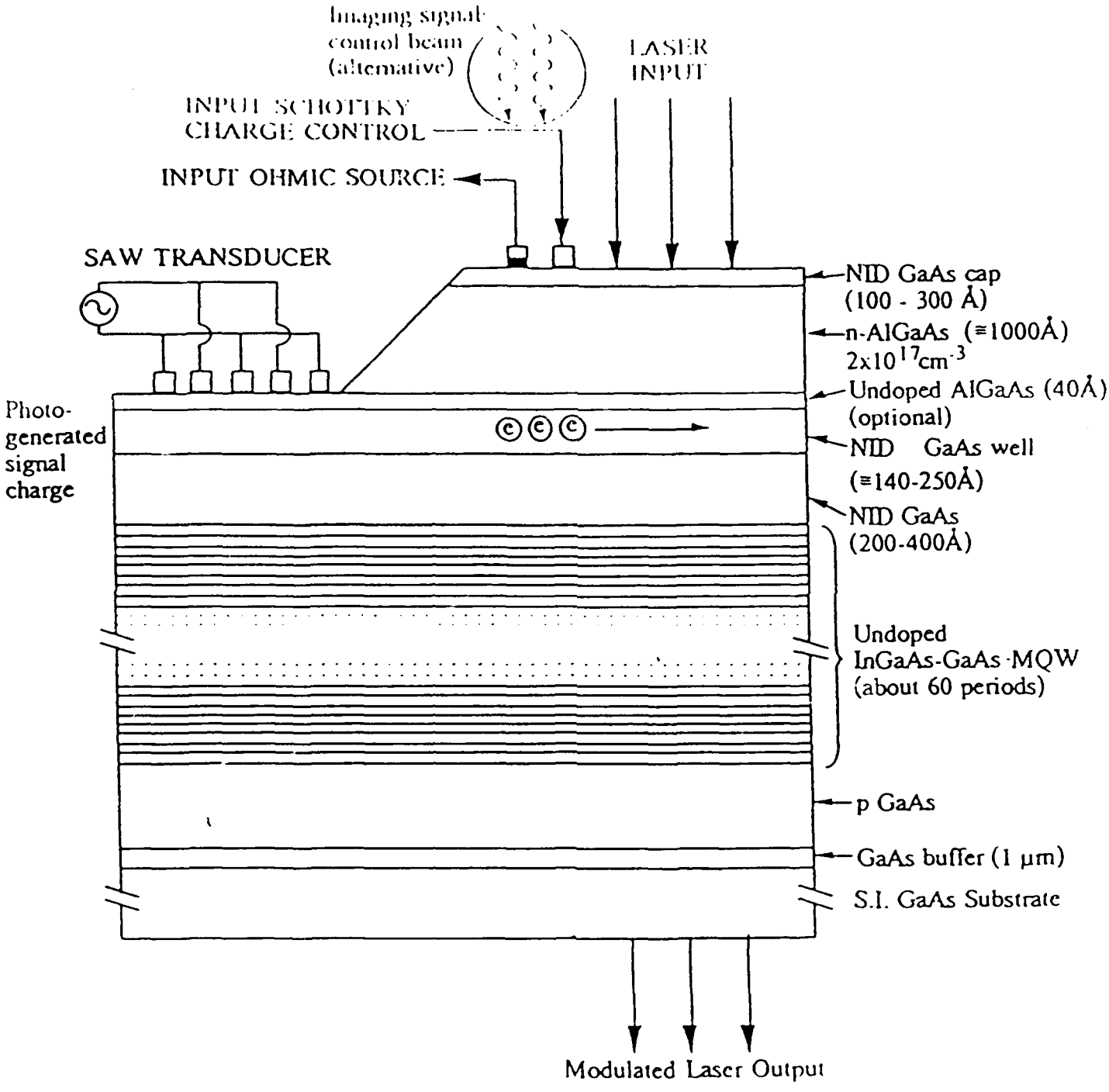

Figure 10

Heterostructure Acoustic Charge Transport (HACT) controlled Multiple Quantum Well optical modulator structure (normal entry)

- Amplitude / phase modulation
- Up to 10 μs delays
- Bandwidth up to 500 MHz

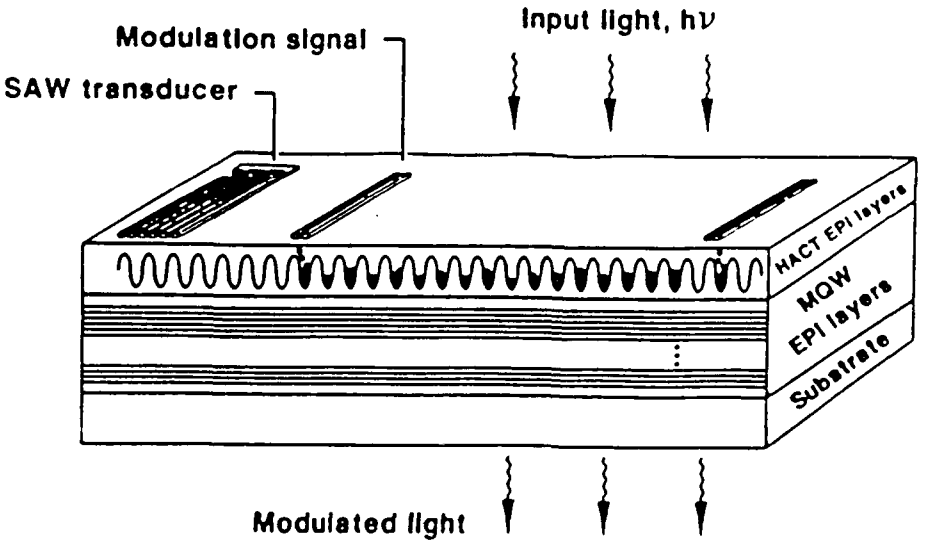

Figure 11

HACT Spatial Light modulator
Single Channel

DEVICE OPERATION - SINGLE PIXEL

Modulation of α and n

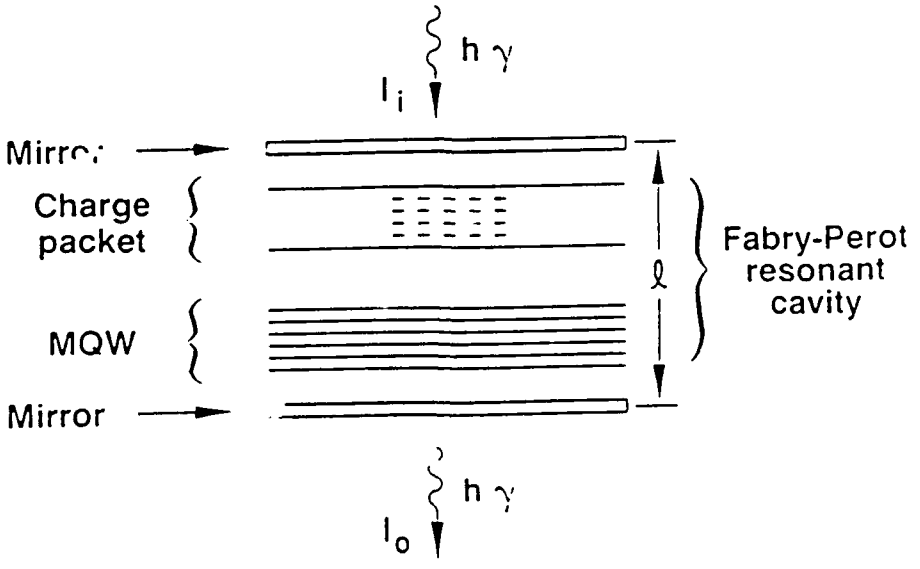

Figure 12

HACT in F-P Cavity for Enhanced Contrast

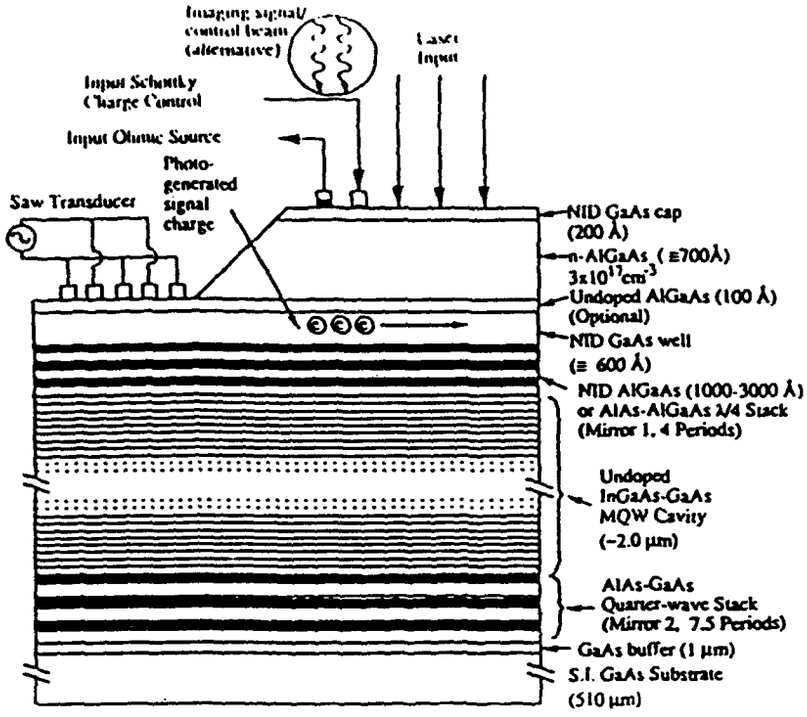

Figure 13

Heterostructure Acoustic Charge Transport (HACT) controlled Multiple Quantum Well optical modulator structure (Reflective Mode).

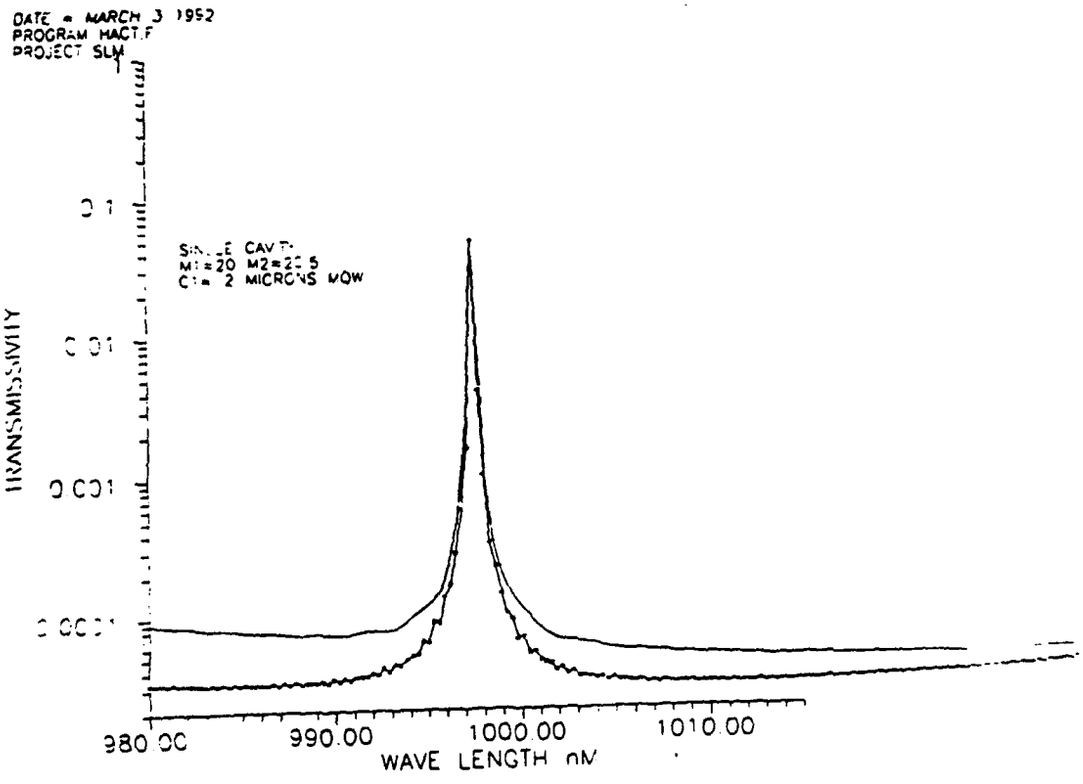

Figure 14

Single Cavity vs Single Cavity with HACT

A.4. Modeling of Contrast Ratio in MQW Cavity Fabry-Perot Modulators

Computer programs were developed for the evaluation of contrast ratio in single and coupled cavity structures consisting of MQW layers. The process involved integration of programs evaluating:

1) Wavefunction and electronic/node energy
2) Optical parameters (λ,n_r) as a Stark effect in MQW layers, and
3) Wave propagation behavior in multi-layered Fabry-Perot structures.

Programs 1 and 2 were developed prior to the ONR/SDIO contract, and software 3 was developed during the course of this work.

A flowchart of the integrated contrast ratio package (KRP) is outlined in Figure 15 .

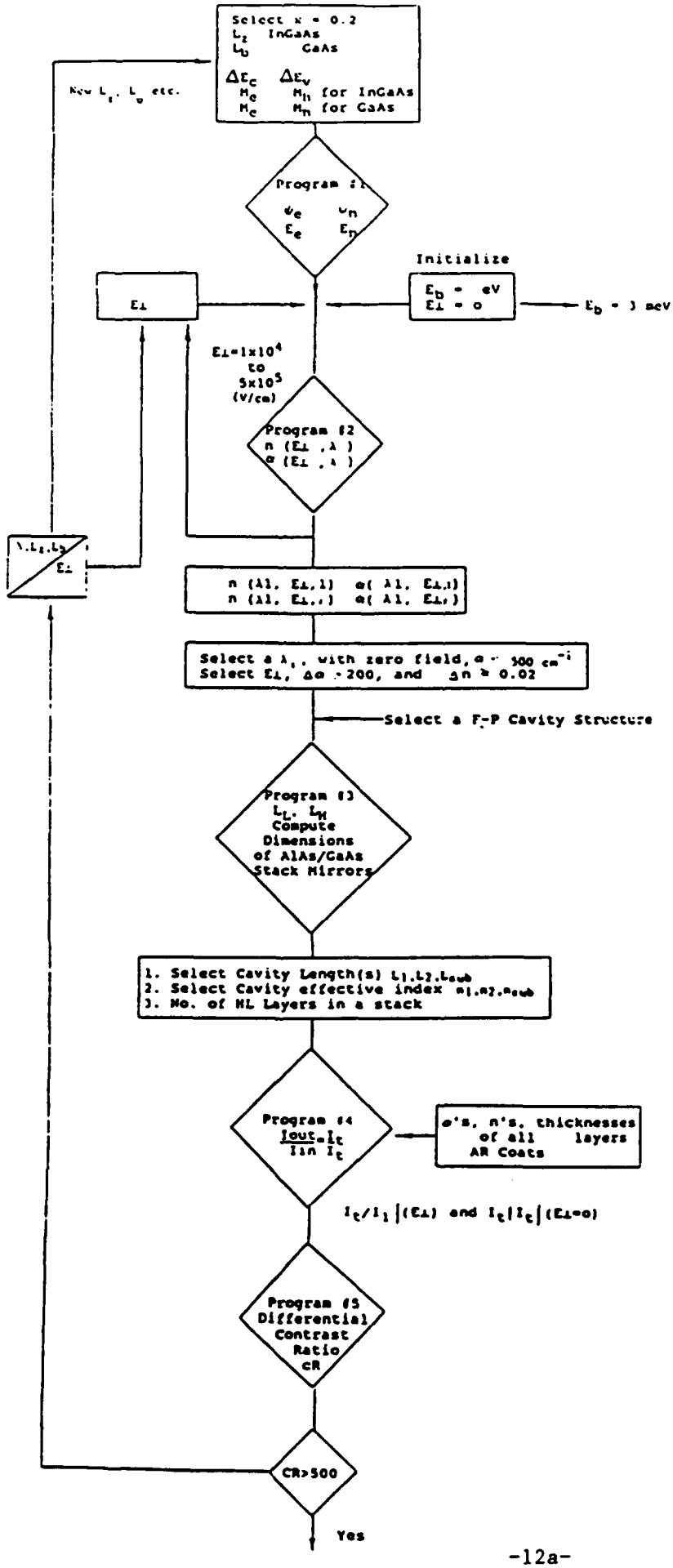

INTEGRATED CONTRAST RATIO PROGRAM

FIGURE 15

A.5. Demonstration of Charge Freezing in HACT Devices

The freezing of signal charge in SAW induced potential wells created in the HACT channel has been used successfully to obtain memory of over 100 μs in a 1 cm long HACT device. The design and performance of the HACT analog memory is described in the attached paper entitled "First HACT Analog Memory Devices Demonstrated (by D. Cullen and M.J. Miller; see appendix).

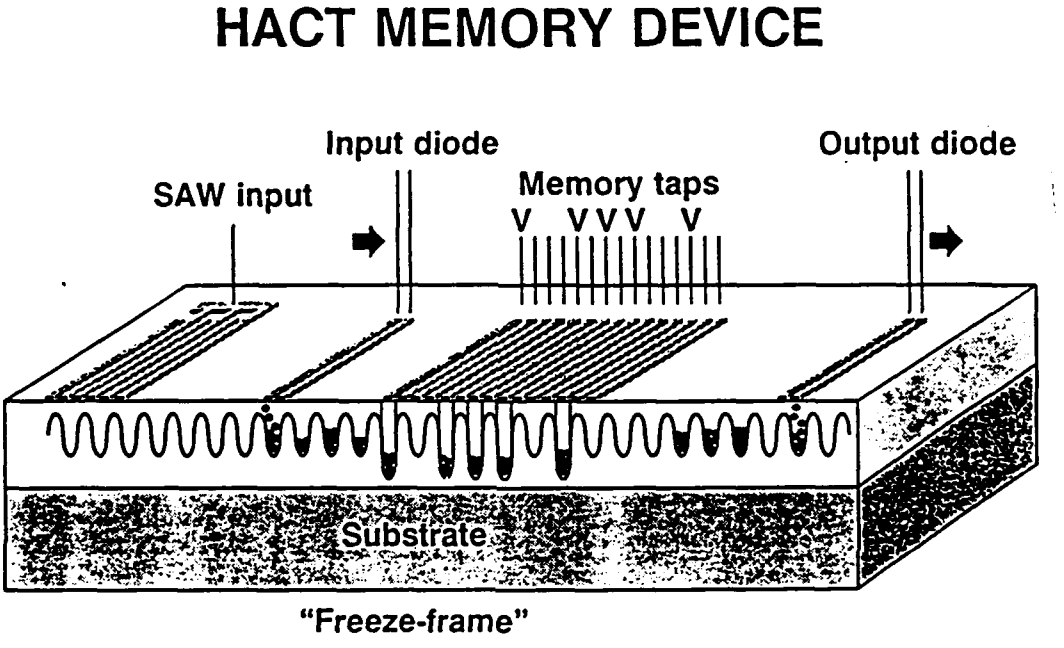

Figure 16

A.6. References

[1] D.S. Chemla, T.C. Damen, D.A.B. Miller, A.C. Gossard, and W. Wiegmann, "Electroabsorption by Stark Effect on Room-Temperature Excitons in GaAs/AlGaAs Multiple Quantum Wells", Appl. Phys. Lett., 42, pp. 864-866, 1983.

[2] T.H. Wood, C.A. Burrus, D.A.B. Miller, D.S. Chemla, T.C. Damen. A.C. Gossard, and W. Wiegmann, "High-speed Optical Modulation with GaAs/GaAlAs Quantum Wells in a P-I-N Diode Structure", Appl. Phys. Lett., vol. 44, pp. 16-18, Jan. 1984.

[3] D.A.B. Miller, D.S. Chemla, T.C. Damen, A.C. Gossard, W. Wiegmann, T.H. Wood, and C.A. Burrus, "Electrical Field Dependence of Optical Absorption Near the Band Gap of Quantum Well Structures", Phys. Rev. B. 32, pp. 1043-1060, July 15, 1985.

[4] Y. Kan, H. Nagai, M. Yamanishi, and I. Suemune, "Field Effects on the Refractive Index and Aborption Coefficient in AlGaAs Quantum Well Structures and their Feasibility for Electrooptic Device Applications", IEEE, J. Quantum Electronics, QE-23, pp. 2167-2179, 1987.

[5] T. Hiroshima, "Electric Field Induced Refractive Index Changes in GaAs - $Al_xGa_{1-x}As$ Quantum Wells", Appl. Phys. Lett. 50, pp. 968-970. 1987

[6] J.S. Weiner, D.A.B. Miller, D.S. Chemla, T.C. Damen, C.A. Burrus, T.H. Wood, A.C. Gossard, and W. Wiegmann, "Strong Polarization Sensitive Electroabsorption in GaAs-AlGaAs Quantum Well Waveguides". Appl. Phys. Lett., 47, pp. 1148 - 1150, 1985

[7] G. Drake, "Effect of Electric Field on the Optical Properties of Semiconductor Quantum Wells", M.S. Thesis (1991), University of Connecticut, Storrs, CT 06268, USA.

[8] D. Marcuse, Theory of Dielectric Optical Waveguides, Academic Press, N.Y., 1991 (Chapter 9).

[9] D.A.B. Miller, J.E. Henry, A.C. Gossard and J.H. English, "Integrated Quantum Well Self Electro-Optic-Effect Device: 2x2 Array of Optically Bistable Switches", Appl. Phys. Lett., 49, pp. 821-873, 1986.

[10] A. Harwit. R. Fernandez, and W.D. Eades, "High Contrast Ratio InGaAs/GaAs Multiple Quantum Well Spatial Light Modulators", SPIE Proc. 1541 [San Diego, CA; July 24, 1991 (to be published)].

[11] R.H. Tan, R.J. Simes, and L.A. Coldren, "Analysis and Design of Surface-Normal Fabry-Perot Electrooptic Modulators", IEEE J. Quantum Electronics, QE-25, no. 11, pp. 2272-2280, Nov. 1989.

[12] K. Hu, L. Chen, A. Madhukar, P. Chen, C. Kyriakakis, Z. Karim and A.R. Tanguay, "Inverted Cavity GaAs/InGaAs Asymmetric Febry-Perot Reflector Modulator", Appl. Phys. Lett., 59, pp. 1664-1666, 1991.

[13] A. Mysyrosicz, D. Hulon, A. Antonetti, A. Migus, W.T. Masselink, and H. Morkoc, "Dressed Excitons in Multiple-Quantum Well Structure: Evidence for an Optical Stark Effect with Femtosecond Response Time", Phys., Rev. Lett., 56, pp. 2748-2751, 1986.

[14] A. Von Lehmen, D.S. Chemla, J.E. Zucker, and J.P., Heritage, Opt. Lett., 11, pp. 609, 1986.

[15] F.C. Jain and K.K. Bhattacharjee, "Multiple Quantum Well Optical Modulator Structures Using Surface Acoustic Wave Induced Stark Effect:, IEEE Photonics Tech. Lett., 1, pp. 307-309, October 1989.

[16] F.C. Jain and K.K. Bhattacharjee, "Multiple Quantum Well Spatial Light Modulator Structures Using Surface Acoustic Wave Induced Stark Effect", SPIE Proc. 1151, pp. 495-506, 1989.

[17] W.D. Goodhue, E.E. Burke, K.B. Nichols, G.M. Metze, and G.D. Johnson, "Quantum Well Charge-coupled Devices for Charge-coupled Device Addressed Multiple Quantum Well Spatial Light Modulators", J. Vac. Sci. Technol, B4, pp. 769-772, 1986.

[18] F.C. Jain and K.K. Bhattacharjee, "Two-Dimensional Spatial Light Modulators Utilizing HACT-Controlled Quantum Confined Stark Effect", SPIE Proc. 1347, pp. 614-622 (San Diego. CA; July 8-10, 1990).

[19] K.K. Bhattacharjee and F.C. Jain, "Spatial Light Modulators Using Acoustic Charge Transport Controlled Stark Effect in Multiple Quantum Well Srructures", 1990 Technical Digest, 14, pp. 64-67, (OSA Topical Conference on Spatial Light Modulators, September 10-12, 1990).

[20] W.J. Tanski, S.W. Merritt, R.N. Sacks, D.E. Cullen, E.J. Branciforte, R.D. Carroll, and T.C. Eschrich, "Heterojunction Acoustic Charge Transport Devices on GaAs", Appl. Phys. Lett., 52, pp. 18-20, January 1988.

[21] D.E. Cullen, T.W. Grudkowski, S.W. Merritt, W.J. Tanski, R.D. Carroll, R.N. Sacks and E.J. Branciforte, "HACT Device Applications", IEEE Ultrasonics Symposium, December 5-7, 1990.

[22] K.K. Bhattacharjee and F.C. Jain, "Multiple Quantum Well Acousto-Optic and Electro-Optic Modulators", IEEE Ultrasonics Symposium, December 4-7, 1990.

[23] Y.J. Ding, C.L. Guo, S. Li, J.B. Khurgin, K.K. Law, J. Stellator, C.T. Law, A.E. Kaplan, and L.A. Coldren, "Observation of Anomalously Large Blue Shift of the Heavy-Hold Photocurrent Peak and Optical Bistability in Narrow Asymmetric Coupled Quantum Wells", Appl. Phys. Lett., 59, pp. 1025-1027, 1991.

[24] C. Sirtori, F. Capasso, D.L. Sivco. A.L. Hutchinson, and A.Y. Cho, "Resonant Stark-Tuning of Second Order Susceptibility in Coupled Quantum Wells', Appl. Phys. Lett., (1991; to be published).

[25] F. Capasso, private communication.

[26] J. He and J. Sapriel, Resonant Acousto-Optical Interaction in Superlattices", Appl. Phys. Lett., 55, pp. 2292-2294, 1989.

[27] V.A. Vyun, Y.O. Kanter, S.M. Kikkarin, V.V. Pnev, A.A. Fedorov, and I.B. Yakovkin, "Acoustoelectric Interactions in GaAs-InGaAs Superlattice", Solid-State Comm. 78, pp. 823-825, 1991.

[28] J.P. van der Ziel and A.C. Gossard, "Optical Birefringence of Ultrathin $Al_xGa_{1-x}As$-GaAs Multilayer Heterostructures", J. Appl. Phys., 49, pp. 2919-2921, May 1978 (also, van der Ziel et al., Appl. Phys. Lett., 28, p. 735, June 1976).

[29] G.J. Sonek, J.M. Ballantyne, Y.J. Chen, G.M. Carter, S.W. Brown, E.S. Koteles, and J.P. Salerno, "Dielectric Properties of AgAs/AlGaAs Multiple Quantum Well Waveguides", IEEE J. Quantum Electronics, 22, pp. 1015-1018, July 1986.

[30] F. Jain, G. Drake, C. Chung, K. Bhattacharjee, and S.K. Cheung, "Two-Dimensional Spatial Light Modulators Using Polarization Sensitive Multiple Quantum Well Light Valve", SPIE Proc. 1564, [San Diego, CA; July 24-26, 1991 (to be published)].

B. Technology Transfer Opportunities

The demonstration of 1200:1 contrast ratio in single cavity Fabry-Perot Structures and the potential of achieving high bandwidths (> 1.0 nm) in coupled-cavity devices have created opportunities for potential technology transfer opportunities for commercial production. In addition, the interest at the Santa Barbara Meeting (August 13-14, 1992) in the electrodeless addressing of HACT-SLMs [which will be fabricated as a part of the new contract (August 8, 1992 - September 30, 1993)] bids well for the commercialization of this technology. In particular, Bell Labs researchers showed great interest in pixel addressing capability of HACT-SLMs for application in SEED based SLMs and other logic systems. We plan to pursue fabrication of this device during the second year.

C. Subcontract to the University of Connecticut

A subcontract was given to the University of Connecticut under the direction of Professor F. Jain. Graduate students who contributed to this project include: C. Cheung, K. Bhattacharjee, S. Cheung, G. Drake, R. LaComb, and P. Dufilie. Messers Bhattacharjee, Chung and Drake completed their doctoral and M.S. thesis during the contract period. Copies of abstracts are attached in the appendix. In addition, a copy of Mr. Glen Drake's Thesis is attached as it involved the calculations of the Stark effect parameters.

Graduate students, Steve Cheung and Ronald LaComb are working towards their Ph.D Thesis which are related to the contract. Mr. Cheung worked over 50% of his time at the United Technologies Research Center (UTRC). Professor Jain spent his sabbatical (May 91 - January 92) at UTRC. Since then he continues spending at least 20% of his time at UTRC.

D. Research Papers

1. F.C. Jain, K.K. Bhattacharjee, and T.W. Grudkowski, "Recent Developments in Multiple Quantum Well Acousto-Optic and Electro-Optic Modulator Structures", Proc. IEEE/UFFS Conference, December 9-11, 1991 (Orlando, Florida). (INVITED PAPER)

2. F. Jain, S. Cheung, G. Drake, C. Chung, and K. Bhattacharjee, "Birefringence Dependent Multiple Quantum Well Light Valves/Modulators and Logic Devices," Proc. of Conference on Emerging Optoelectronic Technologies, December 18-20, 1991 (Banglore, India); SPIE Proc. #1662 (to be published by Tata-McGraw Hill).

3. F. Jain, G. Drake, C. Chung, K. Bhattacharjee, and S. Cheung, "Two-Dimensional Spatial Light Modulators Using Polarization Sensitive Multiple Quantum Well Light Valve," SPIE Pric. 1364 (July 1991 Meeting, San Diego, CA).

4. S. Cheung, R. LaComb, F. Jain, T. Grudkowski, R. Sacks, and G. Drake, "Multiple Quantum Well Optical Modulators", Proc. of CMOC Symposium, March 12-13, 1992 (United Technologies Research Center, E. Hartford, CT). Sponsored by IEEE/LEOS.

5. F.C. Jain, S.K. Cheung, and G. Drake, "Spatial Light Modulators Using Birefringence in Multiple Quantum Well Structures, SPIE Proc. 1751 (July 1992, (to be published)

Work Supported Indirectly

6. F. Jain and C. Chung, "Resonant Tunneling Transistor Lasers: A New Approach in Design Optoelectronically Triggered Lasers and OEICs", Proc. of IEEE Princeton Section Sarnoff Symposium, March 27, 1992. (Given as the opening paper of the conference)

Papers to be Submitted:

7. "High Contrast Fabray-Perot Optical Modulator Using Quantum Confined Stark Effect Tuning in InGaAs-GaAs Multiple Quantum Well Cavity", Applied Phys. Lett.

8. High Contrast Wide Bandwidth Coupled-Cavity Quantum Well Modulators", Applied Phys. Lett.

E. Plans for the 1993

Proposed plan for continued research: The following plan follows a logical approach for achieving a novel HACT 2-Dimensional SLM device having freeze-frame memory capability. No show stoppers are foreseen at present, although the proposed development should be considered as a high risk/highpayoff program.

Phase 2: 1 year, Requires increased level of effort than Phase 1.

	Name of Graduate Student	Degree	Thesis
1.	G. Drake	M.S.	"Effect of Electric Field on the Optical Properties of Semiconductor Quantum Wells"
2.	K. Bhattacharjee	Ph.D.	"Electro-optic and Acousto-Optic Multiple Quantum Well Modulators"

1) Continue optimization of single cavity and coupled cavity Fabry-Perot resonators to achieve 10,000:1 contrast ratio. Demonstrate voltage tunability of the high contrast ratio structures.

2) Fabricate HACT single channel SLM structures. Integrate single cavity resonators onto the HACT device, under the active HACT charge transfer layers. Study the effects of the added layers on the basic HACT charge transfer efficiency and on the optical modulation.

Plans for 1994+

Phase 3:

3) Fabricate and test integrated high contrast ratio resonators onto HACT devices. Test techniques will require pulsed laser operation and stable optics.

4) Demonstrate 2-D HACT SLM operation.

Phase 4:

5) Integrate HACT memory structures first in 1-D than in 2-D.

APPENDIX A

ELECTRO-OPTIC AND ACOUSTO-OPTIC MULTIPLE QUANTUM WELL DEVICES

Kushal Kumar Bhattacharjee

M.S., Indian Institute of Technology, New Delhi, 1978
M.S.E.E, Rensselaer Polytechnic Institute, 1984

A Dissertation

Submitted in Partial Fulfillment of the

Requirements for the Degree of

Doctor of Philosophy

at

The University of Connecticut

1991

ELECTRO-OPTIC AND ACOUSTO-OPTIC MULTIPLE QUANTUM WELL DEVICES

Kushal Kumar Bhattacharjee, Ph.D.

The University of Connecticut, 1991

Electro-optic and acousto-optic Multiple Quantum Well (MQW) devices utilizing Quantum Confined Stark Effect (QCSE) are proposed and analyzed. The emphasis is placed on Bragg type grating structures.

A comb structure realized on the AlGaAs/MQW/AlGaAs type symmetric waveguide in the P-i-N configuration is analyzed at an operational wavelength of 0.885 μm. At this wavelength, with a detuning of 400 Å from the excitonic absorption peak, the loss due to optical absorption is about 3dB/100μm. It is shown that the change in the effective refractive index of the waveguide is substantially higher than a comparable AlGaAs/GaAs/AlGaAs structure. A diffraction efficiency of 100% is achieved at an applied reverse bias of -8.6 Volts for an interaction length of 100 μm.

A surface interdigital structure on an MQW/AlGaAs asymmetric waveguide is considered. Though the change in the effective refractive index is not as drastic as the P-i-N case, due to the exponentially decaying nature of the electric field, considerable improvement over conventional GaAs/AlGaAs type structures is expected.

K.K. Bhattacharjee--The University of Connecticut, 1991

The interaction of guided acoustic wave with light in an asymmetric structure is discussed. The contribution to the change in effective refractive index due to the surface ripple effect and the electro-optic interaction between the electric field accompanying a Surface Acoustic Wave (SAW) and light are estimated. A general scheme for the calculation of elasto-optic contribution is also outlined.

A novel type of Spatial Light Modulator (SLM) utilizing Heterojunction Acoustic Charge Transport (HACT) controlled Stark effect is proposed. Simple calculations support the feasibility of incorporating such structures in 1-D and 2-D SLMs.

Experimental results on the electrical performance of Surface Acoustic Wave delay lines and resonators on MQW/GaAs substrate are presented.

APPENDIX B

IEEE 1991 ULTRASONICS SYMPOSIUM

PROCEEDINGS

B. R. McAvoy
Editor

Sponsored by the
ULTRASONICS
FERROELECTRIC
AND FREQUENCY
CONTROL SOCIETY

December 8 - 11, 1991
Hilton Hotel
at
Walt Disney World Village
Lake Buena Vista, Florida

Vol. 1

91CH3079-1
ISSN: 1051-0117

RECENT DEVELOPMENTS IN MULTIPLE QUANTUM WELL ACOUSTO-OPTIC AND ELECTRO-OPTIC MODULATOR STRUCTURES

F. C. Jain[(1)], K. K. Bhattacharjee[(2)], and T. W. Grudkowski[(3)]

(1) ESE Department, University of Connecticut, Storrs, CT 06269-3157
(Sabbatical Address: UTRC, East Hartford, CT 06108)
(2) Electronics Systems Group, TRW, Redondo Beach, CA 90278
(3) United Technologies Research Center, East Hartford, CT 06108

Abstract

Optical modulators based on acousto-optic and electro-optic effects in multiple quantum well (MQW) and superlattice structures are reviewed. In the case of MQW layers the primary mechanism used is the Quantum Confined Stark Effect (QCSE). Modulators utilizing enhanced changes in optical parameters such as absorption, index of refraction, and birefringence due to externally applied or induced electric fields in AlGaAs-GaAs and InGaAs-GaAs structures are described. In particular, various type of MQW Bragg devices, HACT (Heterostructure Acoustic Charge Transport) modulators, and birefringent light valves are discussed from theoretical and experimental view points. In addition, modulators based on Acousto-Optic effects in superlattices are reviewed. The application of modulators in the realization of subsystems such as of two-dimensional spatial light modulators (SLMs) and optical correlators is also presented.

I. Introduction

Multiple Quantum Wells (MQWs) and superlattices are known to exhibit enhanced electro-optic and acousto-optic effects. This paper reviews the recent developments in the design of MQW modulators. In particular, the emphasis is on the usage of Quantum Confined Stark Effect (QCSE) in MQW based structures. Since the report of excitonic electroabsorption by Chemla et al. [1], Wood et al. [2] and Miller et al. [3], there has been an intense investigation involving QCSE in multiple quantum wells. The two-dimensional confinement of excitons, hosted in a well of thickness L_z (with $a_0/2 < L_z < a_0$; a_0 the Bohr radius), leads to the observation of nonlinear optical properties associated with excitons. The excitonic stability in conjunction with the ability of tuning the absorption (or index) as a function of wavelength with the application of an external electric field has been the central idea behind the development of MQW modulators. Reference is made to Miller et al. [3], Kan et al. [4] and Hiroshirma et al. [5] for a detailed theoretical treatment.

The shift in the absorption peak as a function of electric field also results in a corresponding shift in the index peak, as the two are related by the Kramer-Kronig relation. The observation of Weiner et al. [6] , that the electroabsorption in MQW waveguides is polarization dependent, adds another dimension to the usage of MQWs in novel modulator design. That is, a device designer can realize a modulator using changes in: (1) absorption, (2) index of refraction, and (3) polarization as a function of electric field. The methodology used to apply or induce the electric field in MQW layers also distinguishes one modulator structure from the other. Various methodologies are outlined in section III. Bragg MQW modulators using electro-optic and acousto-optic effects are also discussed.

Recent developments involving coupled quantum wells to shape the electron (and/or hole) wavefunctions to enhance nonlinearities are described. Both inter-band (excitonic) and inter-subband transitions are treated. Acousto-optic effects and polarization dependent nonlinearities in superlattices have attracted several investigations, however they are not reviewed here in any detail.

II. Nonlinear Optical Effects in MQW Layers

The imaginary part of the dielectric constant $\varepsilon_i(\hbar\omega)$, involving excitonic transitions in MQW layers, is given by [4, 7]:

$$\varepsilon_i = (C/L)\left|\int \psi_e(x)\,\psi_h(x)\,dx\right|^2 \cdot F(\hbar\omega_{ex} - \hbar\omega) \qquad (1)$$

and

$$C = [2\pi e^2/\varepsilon_0 m_0^2\omega^2] \cdot |M_b|^2 \cdot |\phi_{ex}(0)|^2 \qquad (2)$$

where $\phi_{ex}(x)$ is the exciton wave function, $\hbar\omega_{ex}$ is the exciton energy, F is the Gaussian line shape function, ψ_e, ψ_h are electron and hole wavefunctions, respectively, L

0051-0117/91/0000-0529 $1.00 © 1991 IEEE

is the width of quantum well, ε_0 is free space permittivity, m_0 is the electron rest mass and M_b is the Block matrix element [3,7]. Using the Kramer-Kronig relation, we can express the real part $\varepsilon_r(\hbar\omega)$ as:

$$\varepsilon_r(\hbar\omega) = 1 + (2/\pi)\, P \int_0^{\infty} [\omega' \varepsilon_i(\omega')\, d\omega'] / [\omega'^2 - \omega^2] \qquad (3)$$

here P is the Cauchy principal integral. The complex index of refraction n_c ($= n - i\kappa$) is related to the complex dielectric constant. Thus, n and κ can be evaluated form ε_r and ε_i. κ is related to the absorption coefficient by:

$$\alpha(\hbar\omega) = 4\pi\kappa / \lambda_0 \qquad (4)$$

As the electric field is applied across the MQW layers, the electron and hole wavefunctions (ψ_e and ψ_h) change. This results in variation of α and n, which are commonly referred as Stark shifts. Generally, the change in n due to the electric field E is expressed as:

$$\Delta n = -(1/2)\, n^3\, [rE + s\, E^3] \qquad (5)$$

where r and s are linear and quadratic electro-optic coefficients. Fig. 1. depicts a typical plot showing the relative contributions of the linear and quadratic (excitonic) effects in the AlGaAs-GaAs MQWs layers. Alternately, the nonlinear effects can be expressed in terms of susceptibility χ [8]. The third order effects which occur in fibers and in MQWs involving inter-subband transitions are expressed using the nonlinear refractive index $\hat{n}$ as [8]:

$$D = \hat{n}^2\, \varepsilon_0\, E \qquad (6)$$

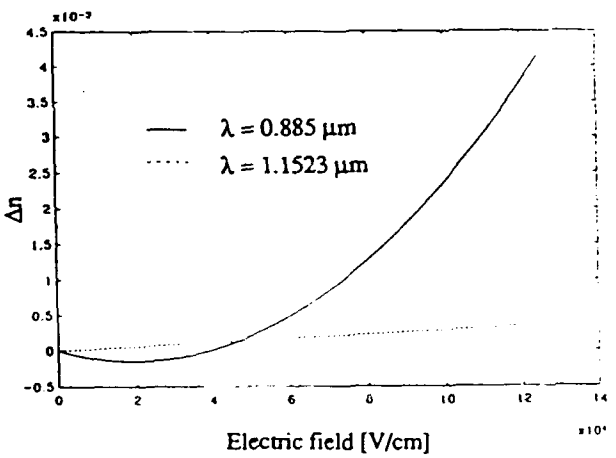

Fig. 1. The variation of refractive index as a function of the applied electric field.

The third order nonlinear index is written in terms of susceptibility $\chi^{(3)}$:

$$\hat{n}^2 = n_0^2 + \chi^{(3)} |E|^2 \qquad (7)$$

Eq. 7 is simplified using approximation:

$$\hat{n} = n_0 + \hat{n}^2 |E|^2 \qquad (8)$$

where $\chi^{(3)}$ is related to $\hat{n}_2$ as:

$$\chi^{(3)} = 2\, n_0\, \hat{n}_2 \qquad (9)$$

Similarly, other effects can be expressed in terms of susceptibility.

III. Modulator Structures

In general, a particular application and associated system requirements determine the structure of modulator. First, the primary optical parameter (e.g. α, n, or Δn), which is varied as a function of electric field, is selected. This determines the operating wavelength, and, in turn, dictates the composition of MQW layers. For example, the structure of Self Electro-Optic-Effect Devices (SEEDs) is designed to provide a positive feedback in a circuit consisting of a MQW diode and a resistor, or MQW diode [p^+-i(MQW)-n] and a photodiode circuits [9]. However, in devices employing index or birefringence changes, the operating wavelength is detuned from that of the main absorption peak. This ensures low losses, and is particularly useful in applications (such as Bragg modulators) across the MQW layers where large interaction length (> 100 μm) are involved. The next task is to select the method to be used to impress the electric field. The electric field may be applied in many ways including:

1) use of reverse biased p^+-i-n or metal (Schottky)-i-n interfaces;
2) electric field associated with below exciton energy optical beam (this is also knows as a.c. Stark effect [8, 9]);
3) field induced by a propagating surface acoustic wave (SAW); and
4) field induced by the transport of signal charges in a channel adjacent to the MQW layers hosting the excitons.

Reverse biased p^+-i-n modulators using the electroabsorptive effect have been reported by Wood et al. [2] and others. Generally, the contrast ratio of these devices is small (~ 4:1). With recent advances in strained QW layers, coupled-well InGaAs-GaAs MQW systems have exhibited an improved contrast of 8:1 [10]. The contrast is significantly enhanced by integrating the MQW layers within a Fabry-Perot cavity. Several

investigators [11,12] have demonstrated improved contrasts by using various configurations. Fig. 2 shows schematically a MQW cavity with quarter wave stacks of dielectric mirrors (e.g. AlAs-GaAs). This device can be tuned if the mirrors are doped p- and n-type, respectively, with an reverse biased electric field applied across the MQW layers (e.g. InGaAs-GaAs). The tuning is provided by the change in index Δn due to the Stark effect. Optical switches utilizing changes in index have been proposed by Kan et al. [4].

Mysyrowicz et al. [13] and von Lehman et al. [14] have utilized the electric field associated with an optical beam. This beam has below gap energy and does not interfere with the excitonic effects.

The schematic of a MQW modulator in which the electric field is induced by a propagating surface acoustic wave (SAW) is shown in Fig. 3. The AlGaAs-GaAs Multiple quantum well layers are shown having a AlGaAs confinement layer (underneath) for waveguiding purposes. The magnitude of induced field is in the range of 3-5 x 10^4 V/cm for modest SAW power levels [15,16]. Since the E component decays in the z direction, the MQW layers should be such that their thickness is a fraction of the acoustical wave length

In the figure the SAW is used both to induce the Stark effect shifts in index and to produce a grating as well. Thus a Bragg modulator can be obtained. Fig. 4 shows a schematic of a modulator using signal charge transport $E(Q_{sig})$ in a channel near the MQW layers. The electric field is impressed across the MQW layers by transporting a signal charge Q_{sig} in an adjacent channel. This method is quite promising, and has two major structural configurations: (1) A Quantum Well CCDs and (2) Heterostructure Acoustic Charge Transport (HACT). Goodhue et al. [17] first used the QWCCD to

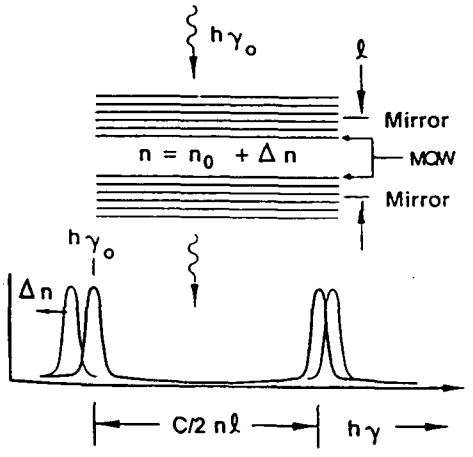

Schematic of a Fabry-Perot Electro-optic modulator.

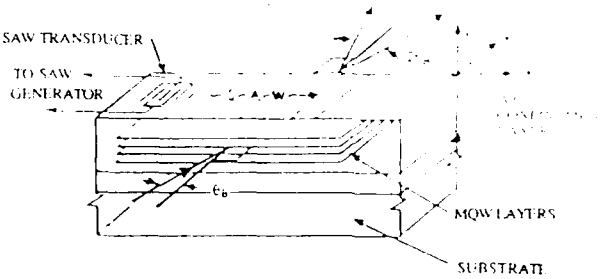

Fig. 3. Schematic of a side entry optical modulator using SAW-Induced quantum confined Stark effect in MQW layers. (This diagram also shows the Bragg type acousto-optic modulator/switch for an incident light beam at Bragg angle Θ_B.)

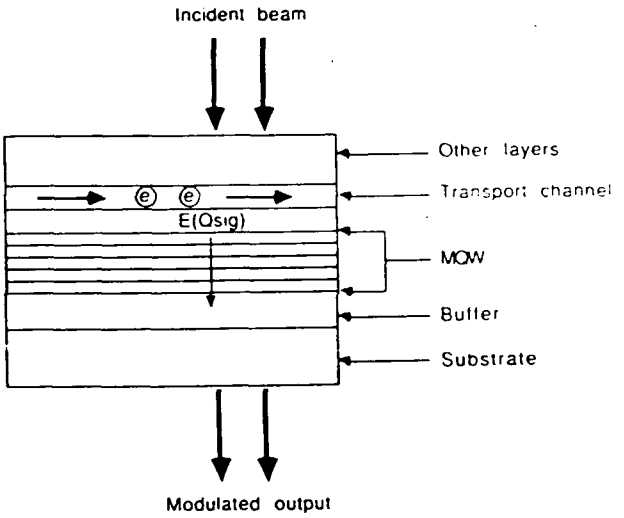

Fig. 4. Schematic of a modulator using signal charge transport in a channel proximaty to the MQW layers.

modulate the excitonic absorption. However, the use of CCD electrodes make it rather complex. HACT modulators, on the other hand, do not require electrodes. Fig. 5 shows a basic HACT modulator [18, 19]. The MQWs are InGaAs-GaAs strained layers; and the HACT part consists of NID (not intentively doped) GaAs (cap) -nAlGaAs (supply) - NID GaAs (transparent and opaque)-NID AlGaAs layers. This permits the use of laser wavelength, λ, which produces excitons in the InGaAs Wells (of MQW layers), without interfering with the transport of electrons in the GaAs channel. The design and operating principle of HACT devices are explained by Tanski et al. [20] and Cullen et al. [21].

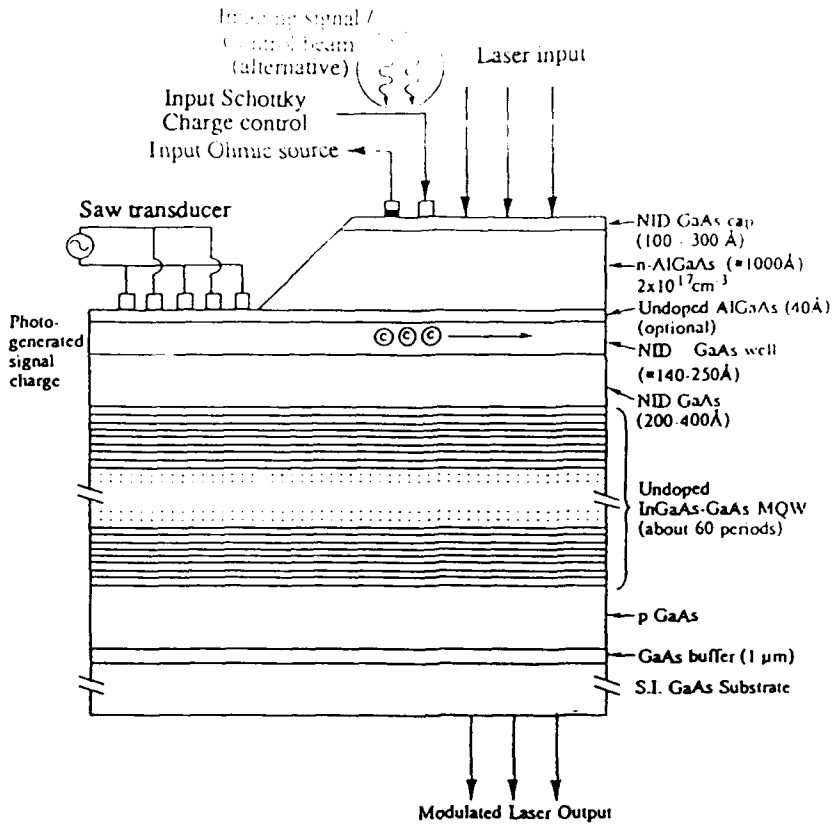

Fig. 5. Heterostructure Acoustic Charge Transport (HACT) controlled Multiple Quantum Well optical modulator structure (normal incident).

A two-dimensional spatial light modulator consisting of multiple channels, with each mesa isolated, is shown in Fig. 6. Each channel has it own signal charge injector and a collector at either end of the channel. All the channels are synchronized by a single SAW transducer (shown at the left end), which, in turn, is synchronized with the laser source.

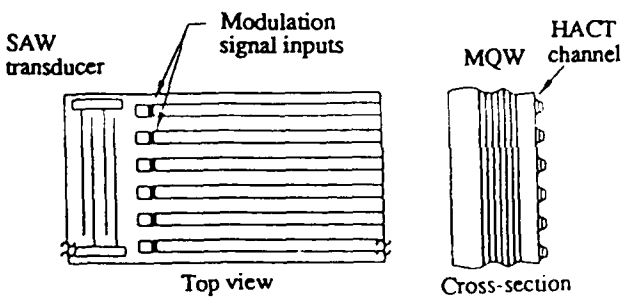

Fig. 6. Potential for about 1000 spots/channel and about 100-1000 channels (10μm x 10μm pixels).

Alternatively, a two dimensional HACT-SLM, having contacts in each pixel, has been described by our group as shown in Fig. 7 [18].

While the electroabsorption due to QCSE in MQWs has been used extensively in modulators, logic devices [e.g. SEEDs], and other applications, the use of index associated effects such as index change and field-dependent birefringence has not been greatly utilized. Kan et al. [4] proposed a switch based on the index change. But the idea was dropped due to associated losses. Our group presented p-i-n Bragg MQW structures [22] which provide high diffraction efficiencies while exhibiting reasonable interaction lengths and losses. These are described in the next section.

The use of field-dependent birefringence in multiple quantum well (MQW) layers [6, 28-29] to implement novel light valves and spatial light modulators has been proposed [30]. The light valve/modulator structures consist of MQW layers located between a polarized-analyzer set in a manner similar to that used in liquid crystal light valves. This is in contrast with conventional Stark effect MQW modulators based on

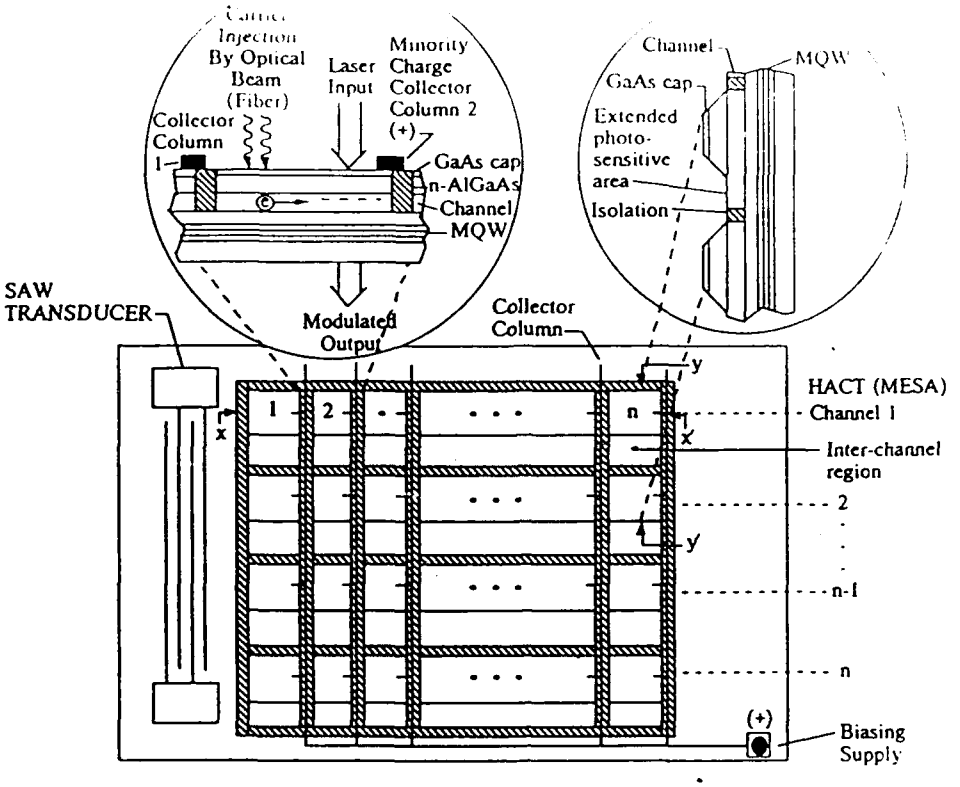

Fig. 7. A two dimensional HACT controlled MQW spatial light modulator with extended photogeneration utilizing the inter-mesa channel.

ectroabsorption. Birefringence values, $\Delta n(E)$, are omputed using experimental absorption data reported the literature [6] for AlGaAs-GaAs MQW layers as a nction of externally applied perpendicular electric ld component $E_\perp$ and the operating wavelength. The efringence can be used in conjunction with the ectroabsorption to enhance the contrast ratio.

Bragg Modulators

gg gratings can be realized either using electro-optic acousto-optic effect. A p^+-i-n AlGaAs-GaAs MQW ucture, using combed p^+ electrode, was analyzed by hattacharjee and Jain [22]. The performance arameters, which include interaction length (100-300 m), PPW, and diffraction efficiency η, look quite romising when compared with conventional GaAs evices. Fig. 8 shows a Schottky grating electro-optic ragg modulator. It is similar to a p^+-i-n Bragg device with the exception that the p^+ layer is substituted by a Schottky comb. The AlGaAs layers form the cladding ayer for the light guided into the MQW layers. The xperimental results showing excitonic shifts are shown Fig. 9. Fig. 10 shows the plot of the diffraction efficiency as a function of the applied voltage for the Schottky structure. A non-intentionally doped top cladding layer of $Al_{0.26}Ga_{0.74}As$ with a thickness of 0.5 μm is assumed. With a background doping level of $10^{15}/cm^3$ the voltage drop across the top cladding layer is about 0.7 V. The MQW region is 0.7 μm thick and a 100 μm interaction length is assumed. The parameters used are [22]: SAW wavelength $\Lambda = 7.0$ μm, interaction length $L = 100$ μm, and $\lambda = 885$ nm.

An alternate scheme is to use the SAW grating for Bragg diffraction. Fig. 3 illustrates such a structure [15]. SAW has two roles in here:

a. it produces a grating, and
b. it induces an electric field to cause Stark shifts (QCSE).

V. Quantum Well Engineering and Wavefunction Shaping

The nonlinear effects can be enhanced by the design of multiple quantum wells. Two commonly methods are: (1) use of strained layers, and (2) the engineering of

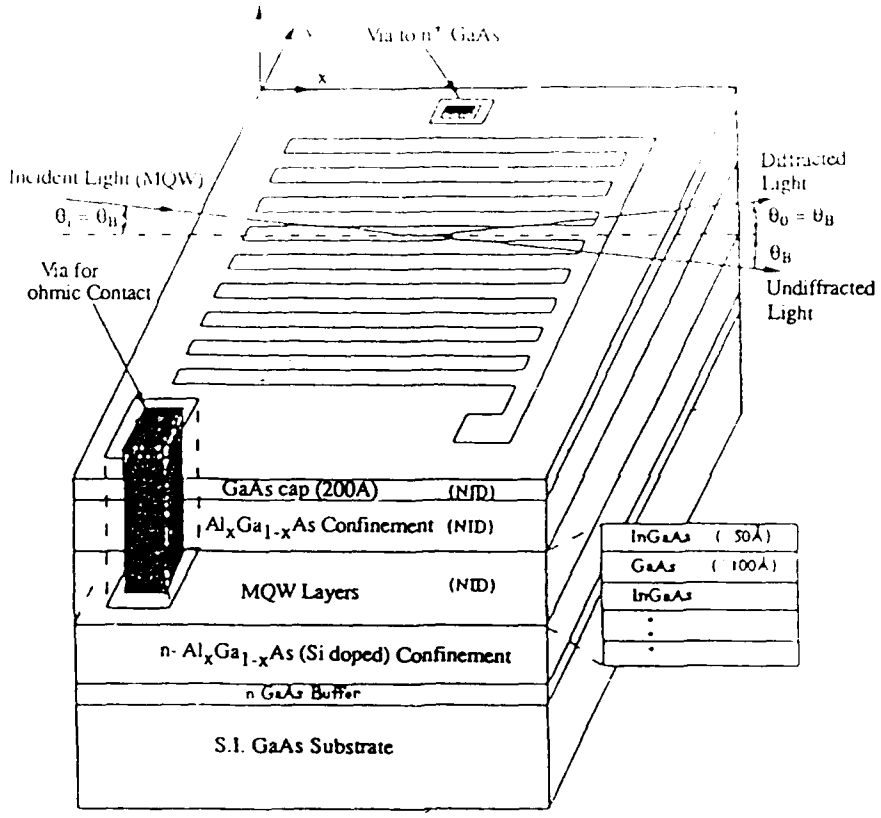

Fig. 8. Schematic of an electro-optic Schottky Bragg Modulator. [The ray path, shown on top of the comb electrode structure, depicts diffraction taking place in the MQW layers (in the x-y plane) between the AlGaAs cladding layers.]

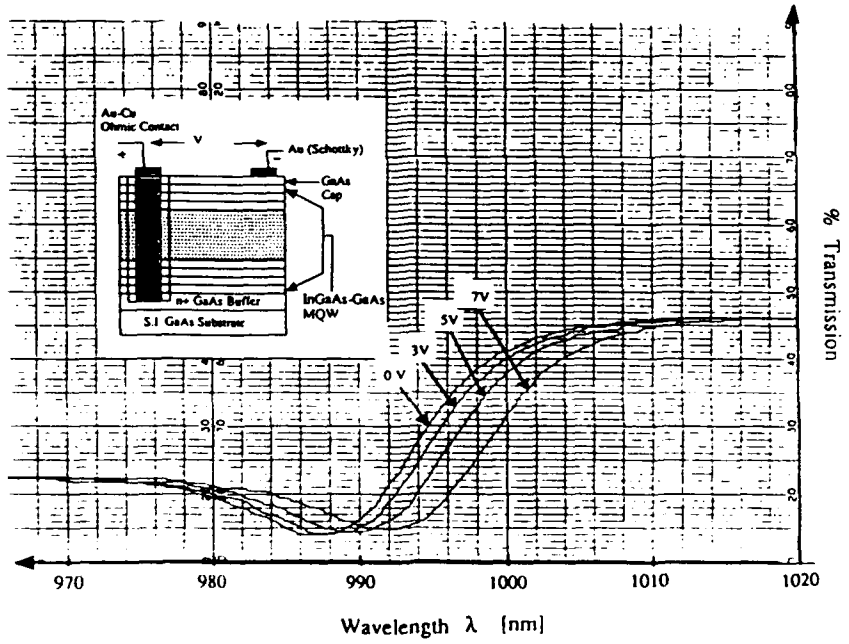

Fig. 9. The measurement of Stark shifts in an InGaAs-GaAs MQW structure (as shown in the inset).

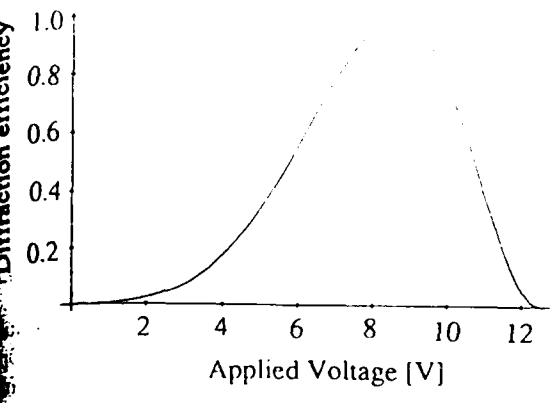

10. Efficiency of the Schottky Bragg Cell with an eraction Length of 100 μm.

pled wells. Harwit et al. [10] and others have shown ter excitonic electroabsorption in coupled wells. is attributed to an increase in the magnitude of the rix element as the electron/hole wavefunctions are lized on one side. Recently, Ding et al. [23] have ined large blue shifts of the heavy-hole photocurrent bistability in asymmetric coupled wells. In addition, asymmetric coupled wells have been used to obtain ond harmonic generation (SHG) using inter-subband itions. This is attributed to an enhanced second r susceptibility [24]. More recently, it has been rted [25] that the use of three barrier coupled wells given substantial improvement in $\chi^{(3)}$, again using subband transitions.

erlattices have also been investigated to enhance sto-optic interactions [26, 27]. He and Sapriel [26] studied resonant acousto-optic effects for elengths near Bragg reflection condition. Vyun et 27] recently reported acousto-electric interaction in s-InGaAs superlattices using surface acoustic waves.

Conclusions

iple quantum well structures offer highly nonlinear cal effects involving excitonic (inter-band) and r-subband transitions. Both categories have been own to exhibit Stark effect tuning. The odulator/SLM structures reviewed in this paper are arily based on excitonic effects which change roabsorption, index of refraction, and birefringence function of the electric field. These phenomena are d individually or in combination to implement odulation. Generally, a Fabry-Perot cavity is used for ance contrast. An important discriminator of device ctures is the way in which the external electric field pplied across the MQW layers hosting the excitions. methods include a.c. Stark effect, SAW pagation, carrier transport in a channel adjacent to the MQW layers and direct application of reverse bias in p-i-n or Schottky configurations.

Bragg Modulators using QCSE have been shown to offer improved interaction lengths (100-200 μm), which is beneficial in the realization of correlators, optical processors and cross-bar switching applications. The recent advances in enhancing QCSE, using wavefunction shaping techniques (coupled wells), further reinforce the advantageous nonlinear properties of these devices.

Acknowledgement

This work has been supported in part by the SDIO/ONR contract, Ct. Department of Higher Education grant and the UCRF grant. Collaboration of Messers C. Chung, S. Cheung, R. LaComb, and P. Dufilie (UConn), and Messers D. Cullen, G. Drake, T. Eschrich, G. Peterson, R. Sacks, W. Tanski, and E. Branciforte is gratefully acknowledged. One of us (FJ) would like to acknowledge the encouragement of Drs. A. DeMaria and A.G. Foyt who facilitated the sabbatical leave at the United Technologies Research Center.

References

[1] D.S. Chemla, T.C. Damen, D.A.B. Miller, A.C. Gossard, and W. Wiegmann, "Electroabsorption by Stark Effect on Room-Temperature Excitons in GaAs/AlGaAs Multiple Quantum Wells", Appl. Phys. Lett., 42, pp. 864-866, 1983.

[2] T.H. Wood, C.A. Burrus, D.A.B. Miller, D.S. Chemla, T.C. Damen, A.C. Gossard, and W. Wiegmann, "High-speed Optical Modulation with GaAs/GaAlAs Quantum Wells in a P-I-N Diode Structure", Appl. Phys. Lett., vol. 44, pp. 16-18, Jan. 1984.

[3] D.A.B. Miller, D.S. Chemla, T.C. Damen, A.C. Gossard, W. Wiegmann, T.H. Wood, and C.A. Burrus, "Electrical Field Dependence of Optical Absorption Near the Band Gap of Quantum-Well Structures", Phys. Rev. B, 32, pp. 1043-1060, July 15, 1985.

[4] Y. Kan, H. Nagai, M. Yamanishi, and I. Suemune, "Field Effects on the Refractive Index and Absorption Coefficient in AlGaAs Quantum Well Structures and their Feasibility for Electrooptic Device Applications", IEEE J. Quantum Electronics, QE-23, pp. 2167-2179, 1987.

[5] T. Hiroshima, "Electric Field Induced Refractive Index Changes in GaAs- $Al_xGa_{1-x}As$ Quantum Wells", Appl. Phys. Lett., 50, pp. 968-970, 1987.

[6] J.S. Weiner, D.A.B. Miller, D.S. Chemla, T.C. Damen, C.A. Burrus, T.H. Wood, A.C. Gossard, and W. Wiegmann, "Strong Polarization-Sensitive Electroabsorption in GaAs-AlGaAs Quantum Well

Waveguides", Appl. Phys. Lett., 47, pp. 1148-1150, 1985.

[7] G. Drake, "Effect of Electric Field on the Optical Properties of Semiconductor Quantum Wells", M.S. Thesis (1991), University of Connecticut Storrs, CT. 06268, USA.

[8] D. Marcuse, Theory of Dielectric Optical Waveguides, Academic Press, N.Y. 1991 (Chapter 9).

[9] D.A.B. Miller, J.E. Henry, A.C. Gossard and J.H. English, "Integrated Quantum Well Self Electro-Optic-Effect Device: 2x2 Array of Optically Bistable Switches", Appl. Phys. Lett., 49, pp. 821-873, 1986.

[10] A. Harwit, R. Fernandez, and W.D. Eades, "High Contrast Ratio InGaAs/GaAs Multiple Quantum Well Spatial Light Modulators", SPIE Proc. 1541 [San Diego, CA; July 24, 1991 (to be published)].

[11] R.H. Yan, R.J. Simes, and L.A. Coldren, "Analysis and Design of Surface-Normal Fabry-Perot Electrooptic Modulators", IEEE J. Quantum Electronics, QE-25, no. 11, pp. 2272-2280, Nov. 1989.

[12] K. Hu, L. Chen, A. Madhukar, P. Chen, C. Kyriakakis, Z Karim, and A.R. Tanguay, "Inverted Cavity GaAs/InGaAs Asymmetric Febry-Perot Reflector Modulator", Appl. Phys. Lett., 59, pp. 1664-1666, 1991.

[13] A. Mysyrosicz, D. Hulon, A. Antonetti, A. Migus, W.T. Masselink, and H. Morkoc, "Dressed Excitons in Multiple-Quantum Well Structure: Evidence for an Optical Stark Effect with Femtosecond Response Time", Phys., Rev. Lett., 56, pp. 2748-2751, 1986.

[14] A. Von Lehmen, D.S. Chemla, J.E. Zucker, and J.P, Heritage, Opt. Lett., 11, pp. 609, 1986.

[15] F.C. Jain and K.K. Bhattacharjee, "Multiple Quantum Well Optical Modulator Structures Using Surface Acoustic Wave Induced Stark Effect", IEEE Photonics Tech. Lett., 1, pp. 307-309 , October 1989.

[16] F.C. Jain and K.K. Bhattacharjee, "Multiple Quantum Well Spatial Light Modulator Structures Using Surface Acoustic Wave Induced Stark Effect", SPIE Proc. 1151, pp. 495-506, 1989.

[17] W. D. Goodhue, E.E. Burke, K.B. Nichols, G.M. Metze, and G.D. Johnson, "Quantum Well Charge-coupled Devices for Charge-coupled Device Addressed Multiple Quantum Well Spatial Light Modulators", J. Vac. Sci., Technol. B4, pp. 769-772, 1986.

[18] F.C. Jain and K.K. Bhattacharjee, "Two-Dimensional Spatial Light Modulators Utilizing HACT-Controlled Quantum Confined Stark Effect", SPIE Proc. 1347, pp. 614-622 (San Diego, CA; July 8-10; 1990).

[19] K.K. Bhattacharjee and F.C. Jain, "Spatial Light Modulators Using Acoustic Charge Transport Controlled Stark Effect in Multiple Quantum Well Structures", 1990 Technical Digest, 14, pp. 64-67 (OSA Topical Conference on Spatial [illegible], Monterey, CA).

[20] W.J. Tanski, S.W. Merritt, R.N. Sacks, D.E. Culler, E.J. Branciforte, R.D. Carroll, and J.C. Eschrich, "Heterojunction Acoustic Charge Transport Devices on GaAs", Appl. Phys. Lett., 52, pp. 18-20, January 1988.

[21] D.E. Cullen, T.W. Grudkowski, S.W. Merritt, W.J. Tanski, R.D. Carroll, R.N. Sacks and E.J. Branciforte, "HACT Device Applications", IEEE Ultrasonics Symposium, December-5-7, 1990.

[22] K.K. Bhattacharjee and F. C. Jain, "Multiple Quantum Well Acousto-Optic and Electro-Optic Modulators", IEEE Ultrasonics Symposium, December 4-7, 1990.

[23] Y.J. Ding, C.L. Guo, S. Li, J.B. Khurgin, K.K. Law, J. Stellato, C.T. Law, A.E. Kaplan, and L.A. Coldren, "Observation of Anomalously Large Blue Shift of the Heavy-Hold Photocurrent Peak and Optical Bistability in Narrow Asymmetric Coupled Quantum Wells", Appl. Phys. Lett., 59, pp. 1025-1027, 1991.

[24] C. Sirtori, F. Capasso, D.L. Sivco, A.L. Hutchinson, and A.Y. Cho, "Resonant Stark-Tuning of Second Order Susceptibility in Coupled Quantum Wells", Appl. Phys. Lett., (1991; to be published).

[25] F. Capasso, private communication.

[26] J. He and J. Sapriel, Resonant Acousto-Optical Interaction in Superlattices", Appl. Phys. Lett., 55, pp. 2292-2294, 1989.

[27] V.A. Vyun, Y.O. Kanter, S.M. Kikkarin, V.V. Pnev, A.A. Fedorov, and I.B. Yakovkin, "Acoustoelectric Interactions in GaAs-InGaAs Superlattice", Solid-State Comm., 78, pp. 823-825, 1991.

[28] J.P. van der Ziel and A.C. Gossard, "Optical Birefringence of Ultrathin $Al_xGa_{1-x}As$-GaAs Multilayer Heterostructures", J. Appl. Phys., 49, pp. 2919-2921, May 1978 (also, van der Ziel et al., Appl. Phys. Lett., 28, p. 735, June 1976).

[29] G.J. Sonek, J.M. Ballantyne, Y.J. Chen, G.M. Carter, S.W. Brown, E.S. Koteles, and J.P. Salerno, "Dielectric Properties of AgAs/AlGaAs Multiple Quantum Well Waveguides", IEEE J. Quantum Electronics, 22, pp. 1015-1018, July 1986.

[30] F. Jain, G. Drake, C. Chung, K. Bhattacharjee, and S.K. Cheung, "Two-Dimensional Spatial Light Modulators Using Polarization Sensitive Multiple Quantum Well Light Valve", SPIE Proc. 1564, [San Diego, CA; July 24-26, 1991 (to be published)].

APPENDIX C

First HACT Analog Memory Devices Demonstrated

D.E. Cullen
United Technologies Research Center
East Hartford, Connecticut 06108

M.J. Miller
Electronic Decisions Incorporated
Urbana, Illinois 61801

Abstract

A new analog memory has been demonstrated using UTRC's heterojunction acoustic charge transport technology. The initial HACT AM's, tested at EDI, had storage time capabilities in excess of 100 usec. The Schottky electrode storage array had 36 memory cells, each cell holding 2 charge packets, giving a maximum signal frequency of half the Nyquist frequency, or 36 MHz. Hold voltages in the 5 to 8 volt range were found to be adequate, and effective storage was obtained at the same dc transport current level that resulted in the best charge transport efficiency. Storage times in the millisecond range are possible with cooling to 0°C. HACT AM's with longer block lengths are presently under development at UTRC.

Introduction

One of the important applications of acoustic charge transport device technology, an analog memory, was described in a 1986 ACT review paper (1). Calculations of storage times, limited by Schottky barrier leakage, indicated the possibility of realizing useful ACT memory devices at room temperature, and devices with greatly enhanced storage capabilities at lower temperatures. Charge storage was demonstrated with experimental ACT devices.

Prior heterojunction ACT technology work at UTRC has been focused on the development of basic HACT technology and on investigating the potential for long (2 to 10 μsec) tapped delay lines. However, encouraged to explore the potential of a HACT memory, several short block length HACT AM devices were recently fabricated and evaluated. The very positive results of this initial investigation, as reported here, have stimulated a wider development effort at UTRC for DoD applications.

Background

Charge storage in an ACT device, conventional or heterojunction ACT, is accomplished in basically the same manner. An array of electrodes on the surface is employed to impose a storage potential on the traveling charge packets. If the storage potential is strong enough to overcome the SAW potential, the charge packets can be stopped and held in position. When the storage potential is removed, the SAW transport of the packets resumes.

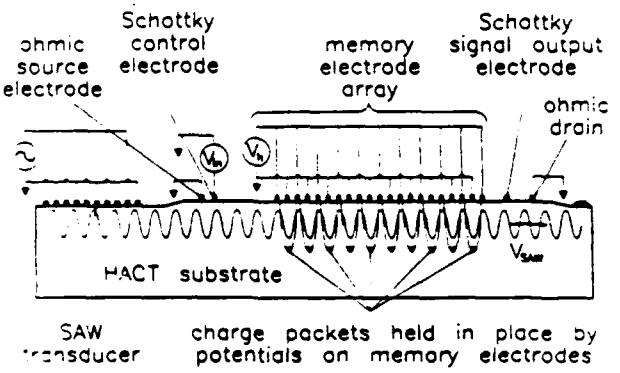

Figure 1 - HACT AM schematic

Figure 1 is a schematic illustration of a simple HACT AM device. Like any HACT device, it contains the following features: 1) an interdigital transducer to generate the SAW which transports the charge packets down the delay path, 2) an input diode with an ohmic electrode which is the source of electrons, and a Schottky electrode which controls the amount of charge in each packet, and 3) an ohmic contact at the end of the delay path to remove the charge from the transport channel. A memory device also has an array of interdigital Schottky electrodes which are used to apply the storage potential, and a Schottky signal output electrode.

In the most general application, the memory array would be designed so that the charge packets could be stored individually giving the AM the same Nyquist frequency (f_n) bandwidth as an HACT delay line. However, this requires a storage electrode array with 2 electrodes per SAW period and therefore comprises an array with the same periodicity as the SAW transducer. In order to avoid the complications, such as SAW reflections and attenuation, that such an array would impose, the first HACT memory devices were designed with a storage array with a periodicity equal to twice the SAW wavelength, λ .

Preprint of paper presented at 1991 IEEE Ultrasonics Symposium, Orlandod Florida, December 8-11

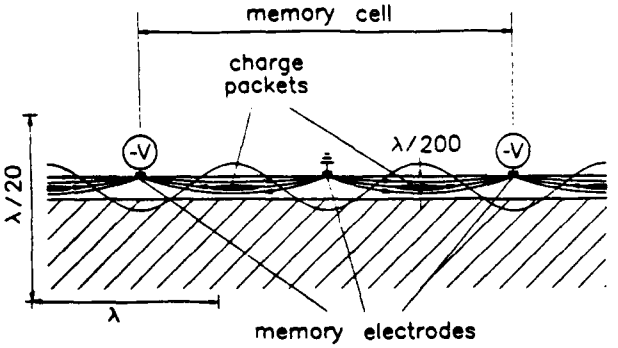

Figure 2 - Geometry of 2 λ memory cell

Figure 2 is a "scale" drawing of the HACT 2 λ memory cell with the vertical scale magnified 20 times the horizontal scale. Charge in a HACT device is transported about 0.1 μm (~ λ/200) from the surface, and it is clear from Fig. 2, that the charge packets are virtually "in line" with the surface electrodes and the electric field that those electrodes generate. A simple model for estimating the minimum hold voltage assumes that the minimum hold field must be at least equal to the maximum SAW field, i.e.,

$$E_{hold} \geq \max E_{SAW},$$

$$\Rightarrow \quad V_{hold} \geq 2\pi\, V_{SAW},$$

which is in good agreement with the experimentally measured 6V minimum hold voltage for a 1V SAW potential. The same model predicts a 3V minimum hold potential for a one-packet-per-cell HACT AM. Since the best AM operation is achieved with storage pulse transition times less than a SAW period, hold pulse rise times of 1 to 2 ns were quite adequate for the 144 MHz devices. This, in addition to the relatively low hold voltage requirements and modest capacitive load presented by the storage electrodes, allowed a conventional laboratory pulse generator to be used for testing.

Charge packets are stored in pairs in 2 λ memory cells and, during the time of storage, the 2 packets can, and will, coalesce. Figure 3 illustrates a time sequence of potential plots showing the SAW, hold, and the SAW + hold potentials in a HACT AM. The first plot, phase = 0, depicts the instant that the hold potential is applied (SAW = 1V, hold = -5V). It is clear that the charge in the 2 packets within the memory cell will merge into 1 packet upon application of the hold voltage. As the SAW continues on, the shape of the SAW + hold potential varies and, at the point where phase = π, there is but 1 well within the memory cell. When the storage potential is removed and the charge is again bunched into 2 packets and carried away by the SAW, the charge in the cell will be divided into 2 packets based upon the charge capacity of the SAW. Information that the packets carried individually is lost. These devices, as a result, have an effective sampling rate of $f_n/2$, rather than f_n in the most general HACT AM.

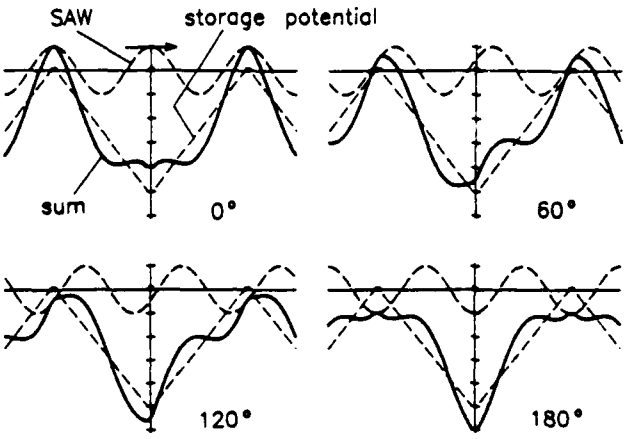

Figure 3 - Time sequence of memory potentials

Experimental HACT AM Devices

The necessary features of a HACT AM device are shown schematically in Fig. 1. Experimental devices were designed with λ = 20 μm SAW transducers which generate a 143.6 MHz SAW (velocity = 2872 m/s). The SAW transports the charge packets down a 30 λ wide mesa etched transport channel. A non-destructive sense electrode, located 100 ns downstream from he input diode and 260 ns from the memory array, was used to examine the input signal. This electrode (NDS #1) is a useful diagnostic feature but not an essential part of the memory device. The memory array consists of 73 interdigitated Schottky electrodes (1 μm wide) with a periodicity of 40 μm, resulting in 36 memory cells. The length of the array was 500 ns making it possible to store a 500 ns long signal. A second NDS electrode (NDS #2), 250 ns downstream of the memory array, served as the signal output electrode. A large area ohmic contact at the end of the transport channel was the return contact for the charge carried by the SAW.

The epilayer configuration of the HACT AM device and the calculated band structure potential were given by Tanski et al. (2) This is the same structure used for HACT tapped delay line devices and is nearly optimal for a GaAs/GaAlAs HACT device. Typical devices yield maximum dc transport currents, I_m, of 70 to 130 μA/mm at a SAW input power level of 1.4 mW/λ (1 V SAW potential in the channel). One hundred μA/mm corresponds to 4.3 million electrons per charge packet per mm width at this frequency. In actual operation, HACT devices are typically biased at an operating point that results in a dc current equal to less than $I_m/2$.

Experimental Results

HACT memory devices were first examined to determine their delay line characteristics to establish bounds and references for subsequent testing as memories. The AM characteristics of: 1) hold voltage requirements, 2) charge storage capacity, 3) leakage current levels, and 4) dynamic range were than determined.

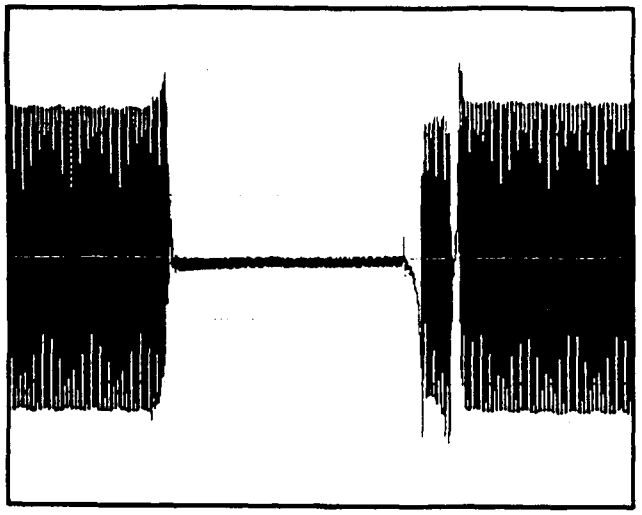

Time (1us/div)

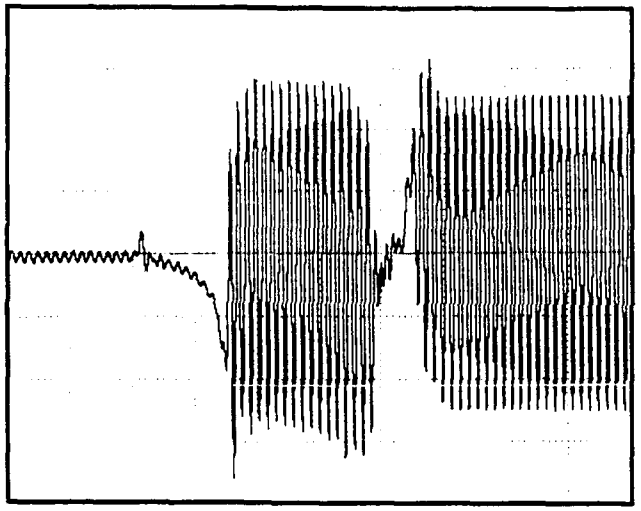

Time (200ns/div)

Figure 4 - NDS #2 output showing 4 μs storage of 36 MHz signal

Operating at the SAW frequency which matches the SAW wavelength to the pitch of the electrodes in the memory array, the maximum useful transport current, I_t was determined. With the device operating as a delay line, I_t was determined by measuring the bandwidth of the device and noting the current level at which the frequency response was reduced by 3 dB. That is roughly equivalent to finding the charge load at which the CTE begins to fall off. The current I_t was measured on typical HACT AM's to be 40 to 50% of I_m, establishing an upper bound on the storage capacity.

The minimum hold voltage is that voltage, which when applied to the memory array, is large enough to overcome the SAW potential and trap and hold the charge packets in place. This voltage was measured by

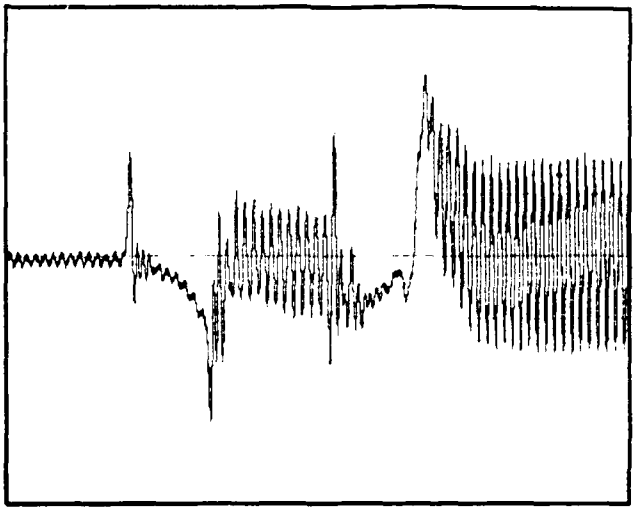

Time (200ns/div)

Figure 5 - NDS #2 output show 100 μs storage of 36 MHz signal

observing the output of NDS #2 in the time domain with a steady single frequency input to the device, and noting the voltage at which storage first occurs. The dc current in this experiment was typically $I_t/10$. For all of the HACT AM's examined, the minimum hold voltage was less than 6 V. The quality of the stored signal improved at hold voltages somewhat above the minimum value. The optimum hold voltage was determined by measuring the frequency response of the stored signal, as it was output from NDS #2, as a function of hold voltage and noting the voltage beyond which there were no further improvements. That voltage was between 5 and 8 V.

Figure 4 is a pair of digital oscilloscope traces of the same NDS #2 output signal, on 0.2 and 1 μs/div time scales, showing 4 μs storage of a 36 MHz signal. The input to the device is continuous, so that the 36 MHz output is seen prior to the application of the storage potential and after the stored signal is read out. The small peak seen in the output approximately 420 ns from the left edge of the 200 ns/div trace indicates the end of the storage pulse. The beginning of the stored signal readout begins approximately 250 ns later, corresponding to the distance between the end of the memory array and NDS #2. The gap in the output between the end of the stored signal readout and the resumption of the delay line characteristic readout is caused by charge redistribution in the region preceding the memory array. Charges tend to pile up in this region when the storage pulse is on and the 36 MHz signal information is lost.

Figure 5 is similar to Fig. 4 except the hold time is 100 μs. The output is seen to be degraded at this point due to leakage from the Schottky memory electrode array. Measurements made on the same devices cooled to 0^{O}C show that reducing the temperature by 25^{O} leads to an increase in the useful hold times by a factor of 5 or more. Recognizable outputs of stored signals, although degraded in quality, were observed at hold times as long

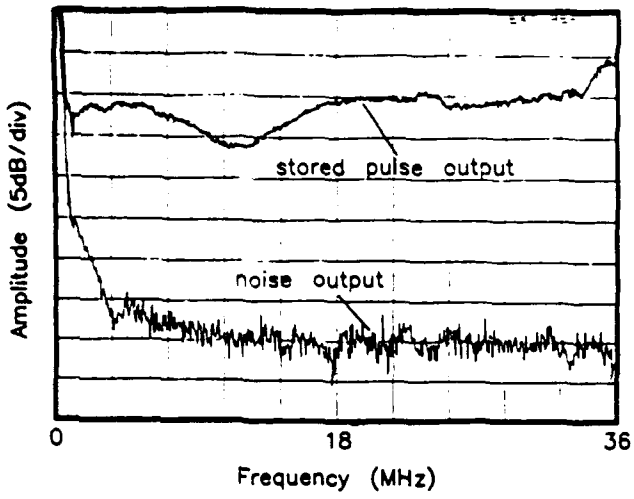

Figure 6 - Frequency spectrum of stored signal

as 500 μs. Cooling to -25°C, readily accomplished with thermoelectric heat pumps, should provide HACT AM hold times in the millisecond range.

Charge storage capacity is defined as the charge load at which the frequency response of the stored signal at $f_n/2$ drops by 1 dB from the value obtained at low charge loads. The output of the stored signal from NDS #2 was gated to remove any direct delay line outputs from the signal presented to the spectrum analyzer. A short storage time of about 100 ns was used in this measurement. Charge storage capacity, measured in this manner, was found to be 1.3 million electrons/packet/mm or approximately 60% I_t. This current level is roughly equal to the current level at which the best delay line operation is obtained with the same device. Thus, functioning as a memory, the HACT device has the same current capacity as the device functioning as a simple delay line.

The maximum useful hold time is limited by leakage of charge into the stationary memory cells. This leakage was measured by biasing the device into cutoff and increasing the hold time until a waveform could be observed in the NDS #2 output. The leakage current can then be calculated and used to determine the fill time, the time it would take to fill the charge packets to the storage capacity. The fill time is approximately 600 μs at room temperature.

The dynamic range of these first HACT AM's, defined here to be the difference between the stored signal output level and the noise output with no ac input signal, was determined from frequency spectrum measurements of the gated output from NDS #2. The noise level was measured with the same dc current level after zeroing the ac input to the device. Figure 6 shows a plot of the frequency spectrum and the noise floor for a 1 μs hold time. The figure indicates a dynamic range of 25 to 30 dB over the $f_n/2$ bandwidth.

Summary

Analog memory devices, based upon HACT technology, have been fabricated, tested, and evaluated. The first HACT AM's, with 0.5 μs block lengths, were found to have a dynamic range of about 30 dB for short hold times, and 100 μs hold times with reduced dynamic range at room temperature. Hold times of nearly 500 μs were observed at 0°C. These initial results have stimulated a larger effort at UTRC to assess the potential of the HACT AM. Longer block length devices with improved leakage characteristics are a near term goal. A design for a 3 μs memory device was recently completed. Modifications to the basic HACT structure to reduce Schottky barrier leakage are being evaluated. Calculations indicate that millisecond AM devices should be possible with cooling to -25°C, and testing of 0.5 μs block length HACT AM devices at low temperatures has been initiated.

Acknowledgments

The authors wish to thank E.J. Branciforte of UTRC for the expert fabrication of the HACT devices, and to R.N. Sacks for the growth of the MBE material. We also acknowledge the encouragement and support of B.J. Hunsinger and R.J. Kansy of EDI, and W.J. Tanski and T.W. Grudkowski of UTRC.

References

1. M.J. Hoskins and B.J. Hunsinger, "Recent Developments In Acoustic Charge Transport Devices", 1986 IEEE Ultrasonics Symposium Proceedings, cat #86CH2375-4, 1986.

2. W.J. Tanski, R.N. Sacks, S.W. Merritt, D.E. Cullen, E.J. Branciforte, T.C. Eschrich, and R.D. Carroll, "Heterostructure acoustic charge transport devices on molecular-beam epitaxy grown GaAs/(Al,Ga)As epitaxial layers", J. Vac. Sci. Technol. B6, 685 (1988).

APPENDIX D

EFFECT OF ELECTRIC FIELD ON THE OPTICAL PROPERTIES OF SEMICONDUCTOR QUANTUM WELLS

Glen William Drake

B.S., University of Hartford, 1982

A Thesis

Submitted in Partial Fulfillment of the

Requirements for the Degree of

Master of Science

at

The University of Connecticut

1991

Table of Contents

List of Tables

List of Figures

A. Introduction

There has been a great deal of interest recently in the properties of semiconductor quantum wells. The need to integrate optical and electronic circuits on single substrates has caused intense study of semiconductor energy band structures which can be engineered and manipulated such as in heterojunctions and quantum wells. Quantum effects have already been used in devices such as semiconductor laser diodes. Many new devices are being developed and proposed which will include quantum well structures including optical modulators, waveguides, and spatial light modulators.

One interesting property of these quantum wells is the existence of excitonic states at room temperature and the shift in energy levels of these states with the application of a perpendicular electric field. This is referred to as the Quantum Confined Stark Effect and it can shift the fundamental absorption edge of the material. Thus, a new means is provided for changing the optical properties of the material. This opens new doors for the integration of optics and electronics on a single substrate. And since the effect is very fast, novel high speed optical modulators, and switches are possible.

Early studies of semiconductor quantum well materials [1] coincided with the development of techniques (primarily molecular beam epitaxy) for growing

high qual..., very thin layers of materials. More recent studies have resulted form the ability to grow V shaped and parabolic shaped potential wells [2][3].

Since the quantum well is a thin, flat, two dimensional structure, it may have applications as a spatial light modulator as well [4].

This thesis gives a method to calculate the effect of electric field on the optical properties (refractive index and absorption) of semiconductor multiple quantum well materials. The calculations are done here for gallium arsenide - aluminum gallium arsenide materials but the method is applicable to other systems as well.

Many papers have been written on methods to calculate electron and hole energy levels and wave functions in bulk and in thin layer materials with and without electric fields applied [1-3, 7, 8, 13]. Other papers describe the existence of room temperature excitonic states in semiconductor quantum wells [5, 12]. Still other papers describe methods of calculating the optical properties of materials given the carrier and hole wave functions and energy levels along with other material parameters.

This thesis attempts to combine much of the above analysis into a productive system for determining the optical properties of a wide variety of quantum well geometries and materials with various fields applied for

use in the design of multi quantum well modulators, detectors, switches, and other integrated optic devices.

An outline of the method used here is shown in the flow chart in figure 1.

To turn the analysis into numerical results much use was made of fairly straight forward computer programs written in Fortran and C, running on common personal computers. The wave function solutions require much use of Airy functions so the core of the computer programs is an Airy function generator.

Other parts of the analysis, the binding energy of excitons, for example, make use of previously published results. References are given as appropriate.

As models are developed they are tested by duplicating the results obtained by others. Once they have been verified in this manner, they are used to calculate the properties of other geometries.

The scope of these studies is fairly large, involving quantum mechanics, solid state physics, optics, and electronics. Some of the processes involved are not clearly understood even today. Clearly there is ample room for continued research in this area and many novel devices could be designed in the future.

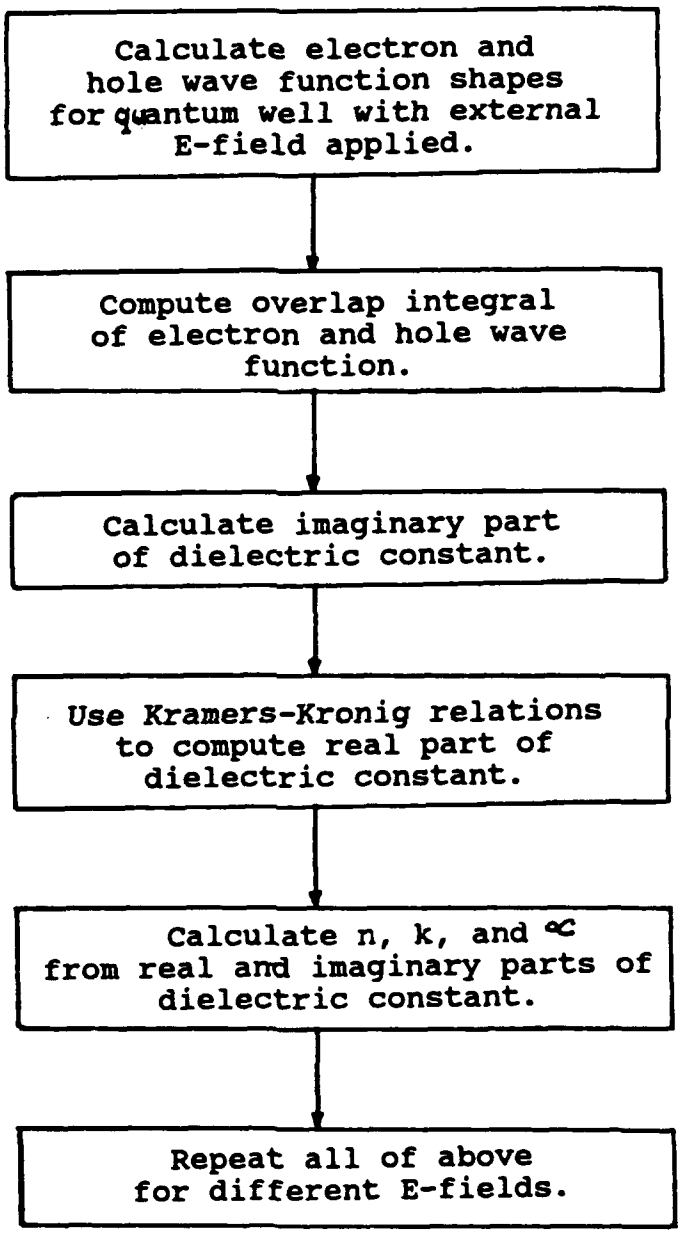

Figure A1: Flow chart for the method used to calculate the optical properties of quantum wells in electric fields.

B. Background

Modern semiconductor growth techniques such as molecular beam epitaxy permit the growth of semiconductors atomic layer upon atomic layer. If several very thin layers are grown with the composition of the layers alternating between higher band gap and lower band gap materials (such as AlGaAs and GaAs), then quantum confinement of electrons and holes can occur in the regions of lower energy called quantum wells (QW's) (Figure B1). This thin layer bandgap engineering allows for many interesting effects and devices based on the two dimensional confinement of quantized states [5]. Quantum Hall effect devices are used as standard resistors at national standards laboratories and quantum well distributed feedback semiconductor lasers are well known.

The quantum wells form a quasi two dimensional barrier for confinement of carriers and classical "particle in a box" analysis can be used to describe the wave functions and quantized energy levels of the electrons and holes. For an infinitely deep rectangular well the wave functions are solutions of the Schroedinger wave equation in one dimension,

$$-\frac{\hbar^2}{2m}\frac{\partial^2\psi}{\partial x^2} + V(x) = i\hbar\frac{\partial\psi}{\partial t} \quad , \qquad \text{(B1)}$$

where $\hbar$ is the reduced Planck's constant, t is time, m is mass, and x is distance.

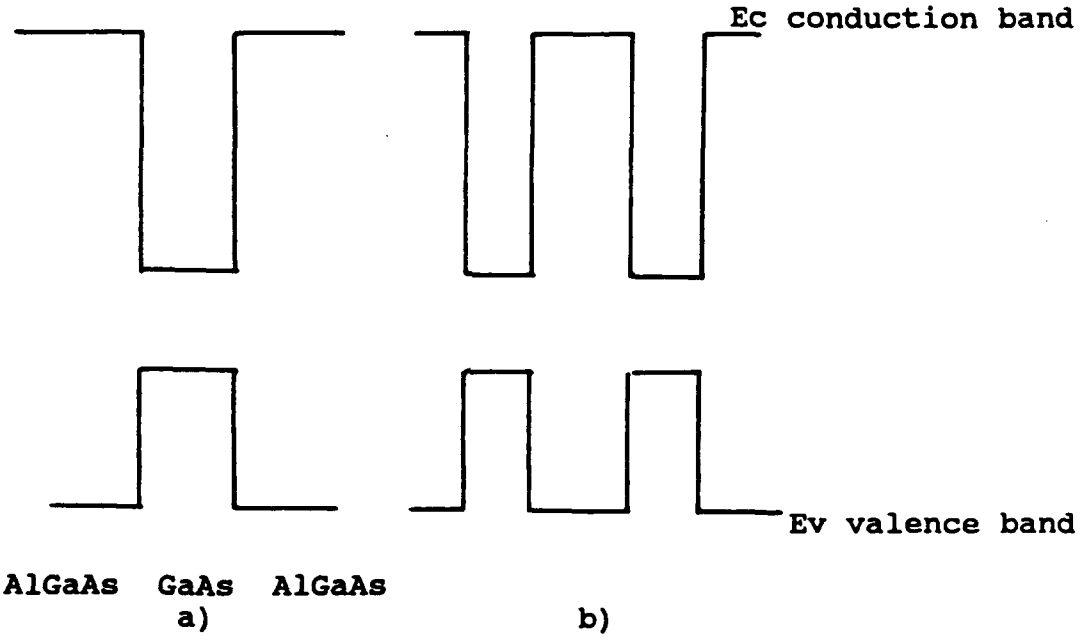

Figure B1. Energy band diagrams for a) quantum well structure, and b) multiple quantum well structure.

If we let V(x), the potential at the bottom of the flat well, be zero then we have solutions of the form,

$$\psi_n(x) = (2/a)^{1/2} \sin(n \pi x/a), \qquad \text{(B2)}$$

with quantized energy levels at,

$$E_n = \frac{n^2 \pi^2 \hbar^2}{2 m a^2} \qquad n = 1, 2, 3 \ldots \qquad \text{(B3)}$$

where a is the width of the well. Figure B2 shows a graphic representation of these classical solutions.

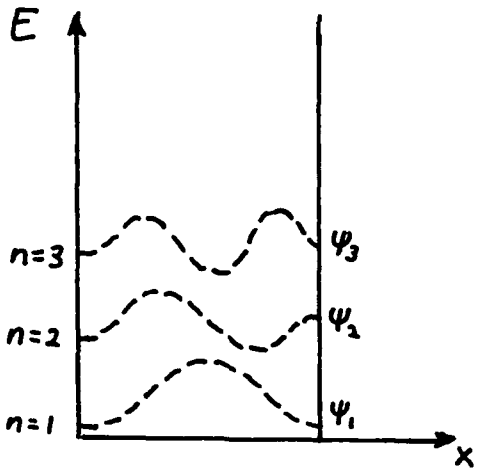

Figure B2. Representation of energy level and wave function solutions for an infinite rectangular potential well.

For a real, finite well the wave functions are actually a little broader and extend beyond the limits of the well. In a multi-quantum well (MQW) structure if the wells are separated enough so that the wave functions from one well to the next do not overlap then the structure can be analyzed as a series of separate quantum wells. If the wave functions do overlap, due to thin AlGaAs barriers (< 100 angstroms) then coupling and resonance effects must be considered. If the barriers are very thin then the wave functions are strongly coupled and a superlattice (a lattice of lattices) is formed.

For the case of an applied electric field the well potential is tilted rather than flat. For this case solutions in the form of Airy functions can be found. This will be shown in detail later. Exact solutions for the case where the well is of finite height have also been found [6]. The tilted potential wells cause the electron and hole wave functions to shift toward opposite sides of the well and cause shifts in the energy levels of the electrons and holes (Fig. B3). The shift in the energy levels is called the Quantum Confined Stark Effect (QCSE) [7].

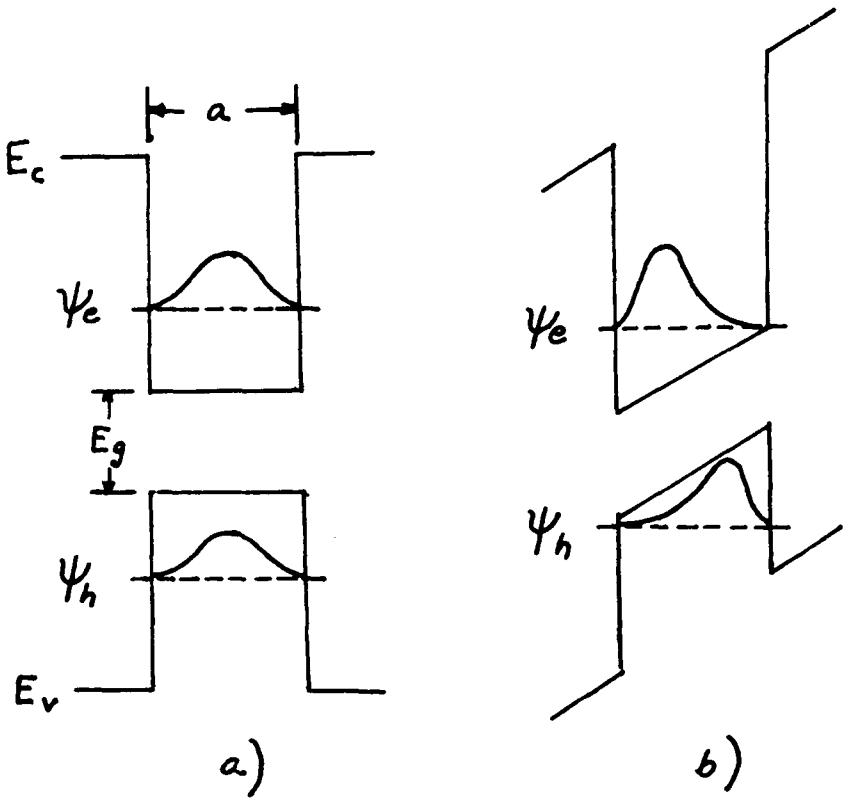

Figure B3. Wave function shapes in a quantum well of width a, a) no perpendicular E-field, b) with perpendicular E-field.

Of particular interest in the study of the effect of an electric field on the optical properties of semiconductor MQW's is the persistent existence of excitonic states in the material due to this quantum confinement. In ordinary bulk semiconductor materials the excitons will exist only at very low temperatures and will disassociate very quickly in the presence of an electric field. However, quantum confined excitons can

exist at room temperature and will not ionize until very high electric fields (> $1x10^7$ V/m) are applied [8].

A comparison must be made between the excitonic effects and the Electro-Optic and Franz-Keldysh effects of electric field on semiconductor optical properties.

The Electro-Optic effect, which is due to distortions in the electron distribution of an optical material when an electric field is applied, has both linear (Pockels) and non-linear (Kerr) components. These distortions change the polarizability, and hence the refractive index of the medium anisotropically. The result is the introduction of new optic axes into the materials.

The change in refractive index as a function of the applied field is of the form,

$$\Delta\left(\frac{1}{n^2}\right) = r\mathcal{E} + P\mathcal{E}^2, \qquad \text{(B4)}$$

where r is the linear electro-optic coefficient (Pockels effect), and P is the quadratic electro-optic coefficient (Kerr effect)[9].

These electro-optic coefficients vary widely from material to material and are very dependent on the axis of the crystal being used. The electro-optic coefficients are small but useable in materials such as lithium

niobate, lithium tantalate, and gallium arsenide for certain orientations.This effect is widely used in integrated optic applications.

The Franz-Keldysh effect is due to band bending generally near the surface of a semiconductor when a depletion region is formed. The bending of the energy bands allows transitions to occur at a lower energy than is possible with no field applied (Fig. B4). The change in energy is related to applied field by [10],

$$\Delta E = (m^*)^{-1/3}(q\,\hbar\,\mathcal{E})^{2/3} \qquad \text{(B5)}$$

where m* is the carrier effective mass, q is the charge of the carrier, $\hbar$ is Planck's constant (reduced), and $\mathcal{E}$ is the magnitude of the electric field.

The maximum ΔE obtained from the Franz-Keldysh effect is in the order of what can be obtained from the Quantum Confined Stark Effect but it is essentially a surface type effect and the ΔE decreases sharply below the surface causing a broadening of the shift. The QCSE, however, is more of a bulk effect in that many layers of quantum wells can be adjoined to increase the total absorption of the device, and there is less broadening of the exciton peak with applied field.

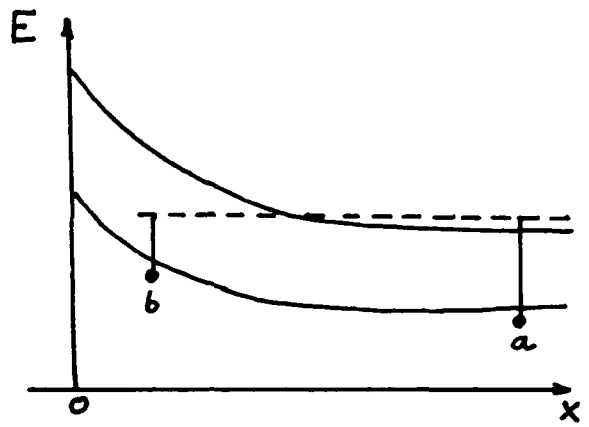

Figure B4. Franz-Keldysh effect; band bending due to E-field across a depletion region can reduce the energy required for a transition (b) compared to the no E-field case (a).

So, compared to other forms of optical modulation, in semiconductors especially, QCSE shows promise due to its speed and the means by which the growth methods allow the engineering of the quantum wells into specific areas of the device.

A brief description of excitons in general follows and then a more detailed description of the method used to calculate QCSE effects on optical properties.

C. Excitons

In general, the term exciton refers to the electronic state resulting from the transfer of an electron from an occupied level in the valence band across the energy gap to an unoccupied level in the conduction band. The energy gap is in the order of a few electron volts so the excitation process is likely to be the absorption of an optical photon.

More specifically, however, the excitons of interest for these calculations are those in which the electron and hole continue to interact with each other forming a hydrogen like state with a certain binding energy that keeps them together. These hydrogen like states may be localized or may travel through the crystal lattice. In quantum well structures, however, their motion will be confined to two dimensions.

Two descriptions of excitons that are often used are the Frenkel and the Wannier exciton models. The Frenkel model assumes weakly interacting atoms in the crystal lattice. The excitation is localized in space, with a spread of a few atomic sites or less. However, in semiconducting crystals the atoms in the crystal lattice interact strongly. Any excitation in this type of lattice will not be localized and will spread out over a large number of atomic sites.

This situation can be modeled by representing the unoccupied state as a positively charged particle called a hole. Thus, the excited state is represented by an electron and a hole interacting with each other in the manner of a hydrogen atom, with the electron and hole orbiting around some common center of gravity determined by the effective masses of the two particles. These states are called Wannier excitons.

For simple spherical energy bands the relative motion of the electron and hole after a direct transition is given by the hydrogen-like wave equation [11]

$$\left[- \frac{\hbar^2}{2m_e^*} \nabla^2 - \frac{\hbar^2}{2m_h^*} \nabla^2 - \frac{e^2}{K_0 r} \right] \psi(r) = \psi(r) \qquad (C1)$$

where K_0 is the static dielectric constant of the crystal and m_e, and m_h are the effective masses of the electron and hole as determined form the conduction and valence band extrema effective masses. The solutions of this equation form a series of discrete levels with energies given by

$$E_{nb} = - R / n^2 \qquad n = 1,2,3 \ldots \qquad (C2)$$

where

$$R = \frac{e^4 \mu}{2\hbar^2 K_0^2} \tag{C3}$$

and μ is the reduced mass of the exciton and is given by

$$\frac{1}{\mu} = \frac{1}{m_e^*} + \frac{1}{m_h^*} \tag{C4}$$

E_{nb} is the binding energy of the exciton and is typically in the order of 4 meV. The total energy of the exciton above the ground state of the crystal is

$$E_n = E_g + E_{nb} \tag{C5}$$

The effect of these excitons on the fundamental absorption edge of the material is an extension if the absorption edge toward lower energies by an amount roughly equal to the binding energy of the exciton.

The spatial extent of the Wannier exciton state relative to a hydrogen atom is given by

$$a_0 = \frac{m}{\mu} K_0 \, a_0^H \tag{C6}$$

where a_0^H is the Bohr orbit radius for the hydrogen atom. The value of a_0 is typically around 150 Å. The Frenkel exciton has a much smaller radius (3 to 7 Å).

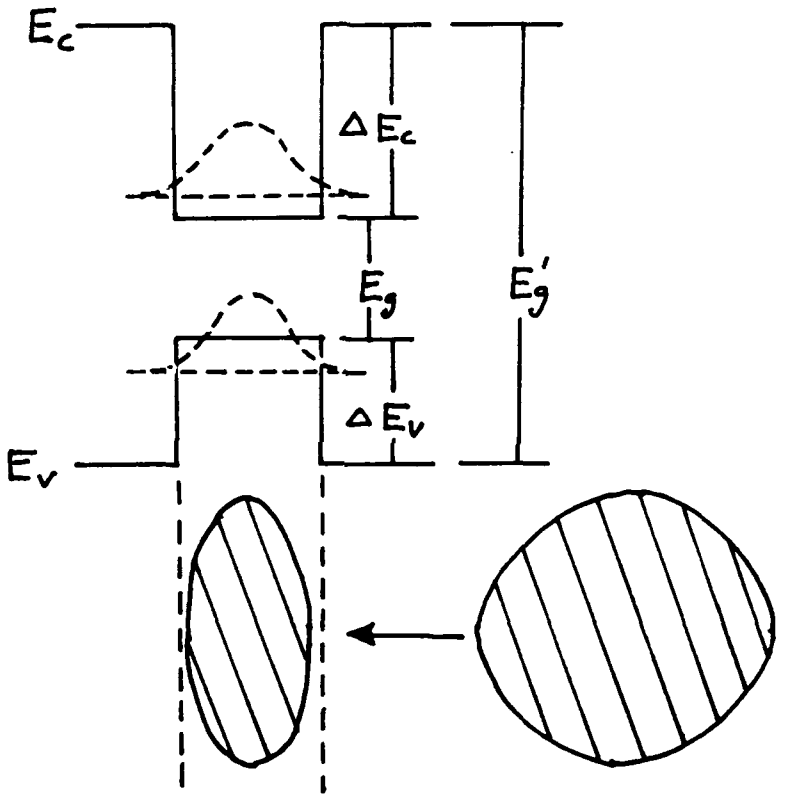

Figure C1. Illustration of multiple quantum well band structure. The dashed lines show electron and hole wave functions. The cross-hatched areas represent a bulk three dimensional exciton and an exciton confined in the quantum well.

Electron hole interaction is shielded in the presence of other free carriers in the system. This is

one of the reasons that excitons are only seen in relatively pure materials or materials at temperatures near absolute zero. However, the presence of quantum wells will enhance the ability of excitons to form due to the two dimensional confinement and resulting increase in oscillator strength.

Figure C1 illustrates the two dimensional confinement of an excitonic state. The state is made possible because in some systems (such as GaAs/AlGaAs) the minimum energy level of the conduction band and the maximum energy level of the valence band occur in the same compound. The excitonic state becomes confined in the potential well, still free to move in the plane of the quantum well layer.

The two dimensional confinement also plays a big part in the effects of electric field on the excitonic states. The field will cause the electron wave function to move toward one side of the quantum well and the hole wave function will be pulled toward the other side. This changes both the magnitude of the excitonic energy level and the probability of interaction between the electron and hole. It is these effects which form the basis for the change in optical properties of the material with application of electric field.

D. Method

The starting point for the analysis is the expression for the imaginary part of the dielectric constant [12]

$$\epsilon_i(\hbar\omega) = \frac{2\pi e^2}{\epsilon_0 m_0 \omega^2 L_z} \frac{3}{2} \left|Mb\right|^2 \left|\phi_{ex}(0)\right|^2 \cdot \left|\int \psi_{e_i}(z)\ \psi_{h_j}(z)\ dz\right|^2 \cdot F(\hbar\omega_{ex} - \hbar\omega) \quad \text{(D1)}$$

where,

e = electronic charge

m_0 = electron rest mass

L_z = thickness of quantum well

ψ_{e_i} = wave function of the ith electron

ψ_{h_j} = wave function of the jth hole

and,

$$\left|M_b\right|^2 = \frac{m_0^2\ E_g\ (E_g + \Delta)}{12\ m_e\ (E_g + \frac{2}{3}\Delta)}$$

which is the average matrix element for the Bloch state. This term is often doubled to give results that compare with experiment.

The final term of equation (D1) is the Gaussian line shape function,

$$F(\hbar\omega_o - \hbar\omega) = \frac{1}{\sqrt{\pi}\delta} \exp\left[-(\hbar\omega_o - \hbar\omega)^2 / \delta^2 \right] \qquad (D2)$$

where,

$$\delta = h/\tau\,(\ln 2)^{-1/2}$$

and τ is the lifetime.

In equation D1 the Gaussian line shape is calculated using $\hbar\omega_{ex} = E_g + E_e + E_h - E_{exb}$ where,

E_g = the band gap energy

E_e = the electron energy

E_h = the hole energy

E_{exb} = the exciton binding energy

From ϵ_i we can get the real part of the dielectric constant using the Kramers-Kronig relation,

$$\epsilon_r = 1 + \frac{2}{\pi} P \int_0^\infty \frac{\omega' \epsilon_i(\omega')\, d\omega'}{[\omega']^2 - \omega^2} \qquad (D3)$$

where P is the Cauchy principal value of the integral. This integral is evaluated numerically.

From the real and imaginary parts of the dielectric constant we can get the refractive index, n, and the extinction coefficient, k, using,

$$n_c = n + ik = \sqrt{\epsilon_r + i\epsilon_i}$$

$$n = \frac{1}{2}\left[\epsilon_r + (\epsilon_r^2 + \epsilon_i^2)^{1/2}\right]^{1/2} \qquad \text{(D4)}$$

$$k = \frac{1}{2}\left[-\epsilon_r + (\epsilon_r^2 + \epsilon_i^2)^{1/2}\right]^{1/2} \qquad \text{(D5)}$$

The absorption is obtained from k using,

$$\alpha = \frac{4\pi k}{\lambda_0} \qquad \text{(D6)}$$

The heart of equation D1 is the overlap integral

$$\int_0^\infty \psi_e(x)\ \psi_h(x)\ dx, \qquad \text{(D7)}$$

with x being the perpendicular distance through the quantum well.

The overlap integral tells the probability of electron-hole interaction. The wave functions $\psi_e(x)$ and

$\psi_h(x)$ are normalized such that the overlap integral is nearly equal to one with no E-field applied since the electron and hole wave function shapes are nearly identical in the zero field case.

As E-field is applied, the electron and hole wave functions separate to opposite sides of the well, this causes the overlap integral to decrease. This will be demonstrated later.

To find the wave functions in the quantum well with E-field applied an infinite well solution to the Schroedinger wave equation

$$-\frac{\hbar^2}{2m}\frac{\partial^2\psi}{\partial x^2} + V(x)\psi = ih\frac{\partial\psi}{\partial t} \qquad \text{(D8)}$$

was used, where V(x) is a linear potential ramp in the region $0 < x < L$ where L is the thickness of the quantum well (Fig. D1).

With a transformation of variables equation D8 can be written as

$$\frac{d^2\psi}{dw^2} - w\psi = 0, \qquad \text{(D9)}$$

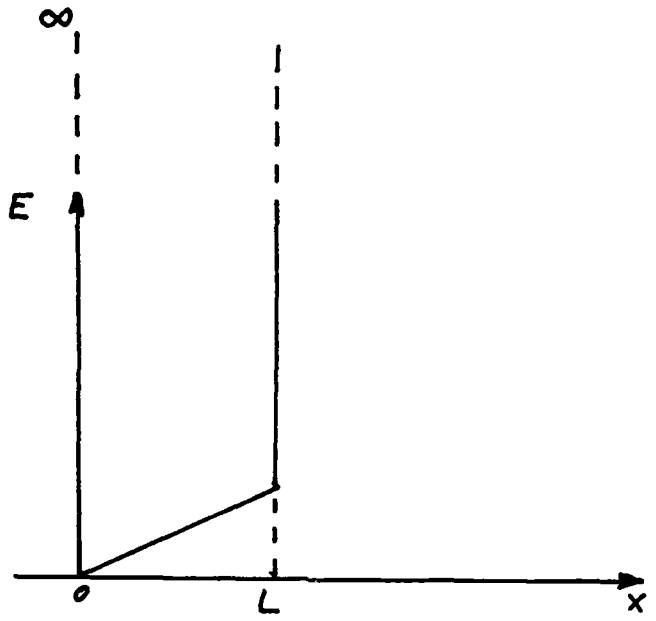

Figure D1. Infinite well approximation.

the solutions to which are in the form of Airy functions. The complete derivation is shown in the next section.

C language computer programs were written to generate the Aires functions and to calculate the wave functions with an applied E-field. Examples of calculated wave function shapes are shown in figure D2.

For the infinite well approximation the wave functions will go to zero at the boundaries of the well. In reality, the well potential is not infinite and the wave functions will tail off beyond the walls of the well. To compensate for this effect the calculations are

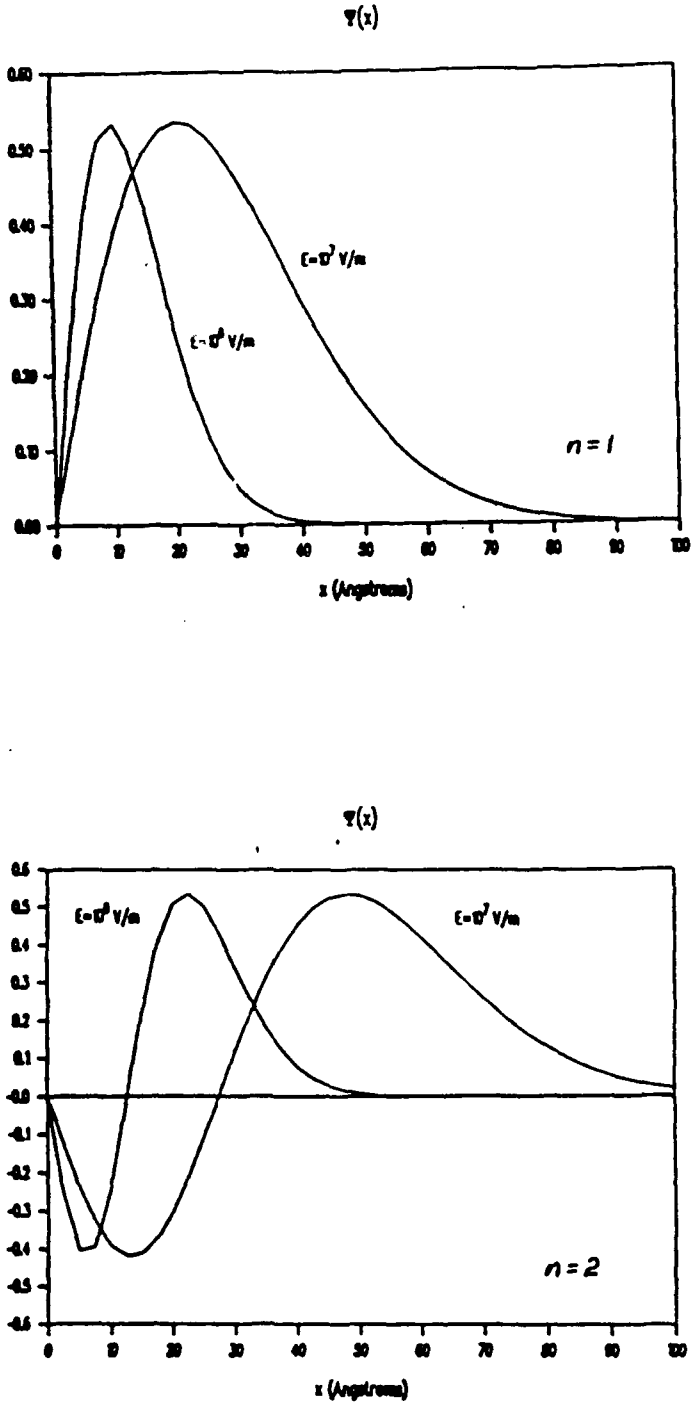

Figure D2. Calculated electron wave function shapes for n=1 and n=2 states with different E-fields applied.

done using a well width that is slightly larger than the actual well width. The effective well width to be used can be determined by a tunneling resonance calculation. In the case of a 100 angstrom well the effective width is calculated to be about thirty percent greater than the actual width of the well.

So, using the effective well width approximation wave functions are generated for the electron and hole of interest. Each of these wave functions is individually normalized and then the two are multiplied together. Integrating the resulting wave function gives the overlap integral.

If the two wave functions are nearly identical, such as for the zero field case, then the overlap integral should come out close to unity. As the E-field is increased the wave functions for the electron and hole move toward opposite sides of the well and the product of the two wave functions becomes smaller making the overlap integral smaller with a lower limit of zero.

Thus, for any given E-field, the overlap integral part of equation D1 simply becomes some number between zero and one. Remember that it is the imaginary part of the dielectric constant that is being calculated. The main effect of the overlap integral on the imaginary part

of the dielectric constant will be to flatten the shape of the curve at higher E-fields.

The shape of the curve itself is determined mainly by the Gaussian line shape function, equation D2. For this calculation the electron and hole energies as well as the exciton binding energy for various applied fields needs to be known. The electron and hole energies can be determined using tunneling resonance computations, the exciton binding energy, however, requires a more complex variational calculation. For this paper published values for these quantities were used. See, for example, reference 8, page 1052.

Still referring to equation D1 and the calculation of the imaginary part of the refractive index, the Gaussian line shape function determines the shape of the curve. Changes in the values of the electron, hole, and exciton binding energies tend to shift the curve up or down in wavelength. Thus, the overlap integral determines the magnitude of ϵ_i and the line shape function and the changes in energy of the exciton states with E-field determine the position of the maximum.

The computational method used was to generate the electron and hole wave functions for a given E-field simultaneously, normalize them and determine the overlap integral numerically. The line shape function was then

calculated using a look up table for the values of Ee, Eh, and Eexb. This generated a data set that represented the imaginary part of the dielectric constant.

The Kramers-Kronig was then performed numerically on this data to generate the real part of the dielectric constant. Then, from the real and imaginary parts of the dielectric constant, the complex refractive index is determined as well as the absorption.

E. Results

The following results were computed for a 100 angstrom GaAs quantum well in AlGaAs. The values and material parameters used are shown in table E1 for the geometry shown in figure E1.

x = mole fraction of Al in AlGaAs = .3

m_e = electron effective mass = $m_0(0.0665 + 0.0835\ x)$

m_{lh} = light hole " " = $m_0(0.094 + 0.043\ x)$

m_{hh} = heavy hole " " = $m_0(0.34 + 0.42\ x)$

τ = 3.69×10^{-13} sec. Ref. 5

Δ = .33eV (for a 60:40 split ratio)

E_g = 1.4 eV

	No Field (meV)	E = 1×10^5 V/cm (meV)
E_e = first electron energy	32	26
E_{lh} = light hole energy	24	17
E_{hh} = heavy hole energy	8	-5
E_{exb} = exciton binding energy	9.5	7.3

λ = exciton radius = 70 Å

Table E1. Values used for computations.

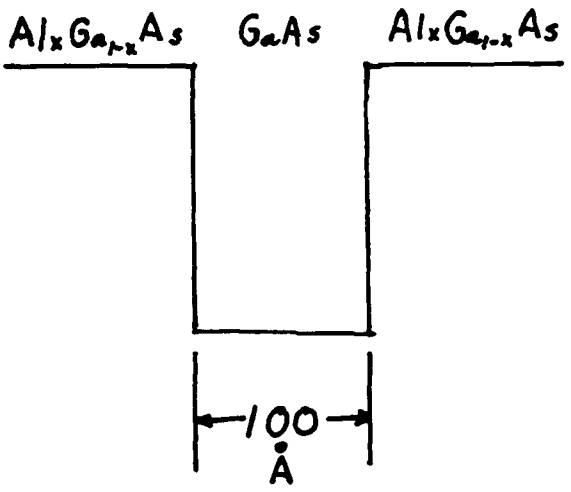

Figure E1. Geometry used for computations.

The particle energy values are shown in the table for zero field and $1x10^5$ V/cm. Values at other E-field values were also used and these were obtained from reference 8 page 1052.

Computed normalized wave functions for the first electron and first heavy hole are shown in figure E2. Also shown is the curve that represents the product of the two wave functions. Integrating this curve gives the overlap integral. Note that as the E-field is increased from $3x10^7$ to $8x10^7$ V/m the electron and hole wave function peaks move away from each other to opposite sides of the quantum well and the product decreases.

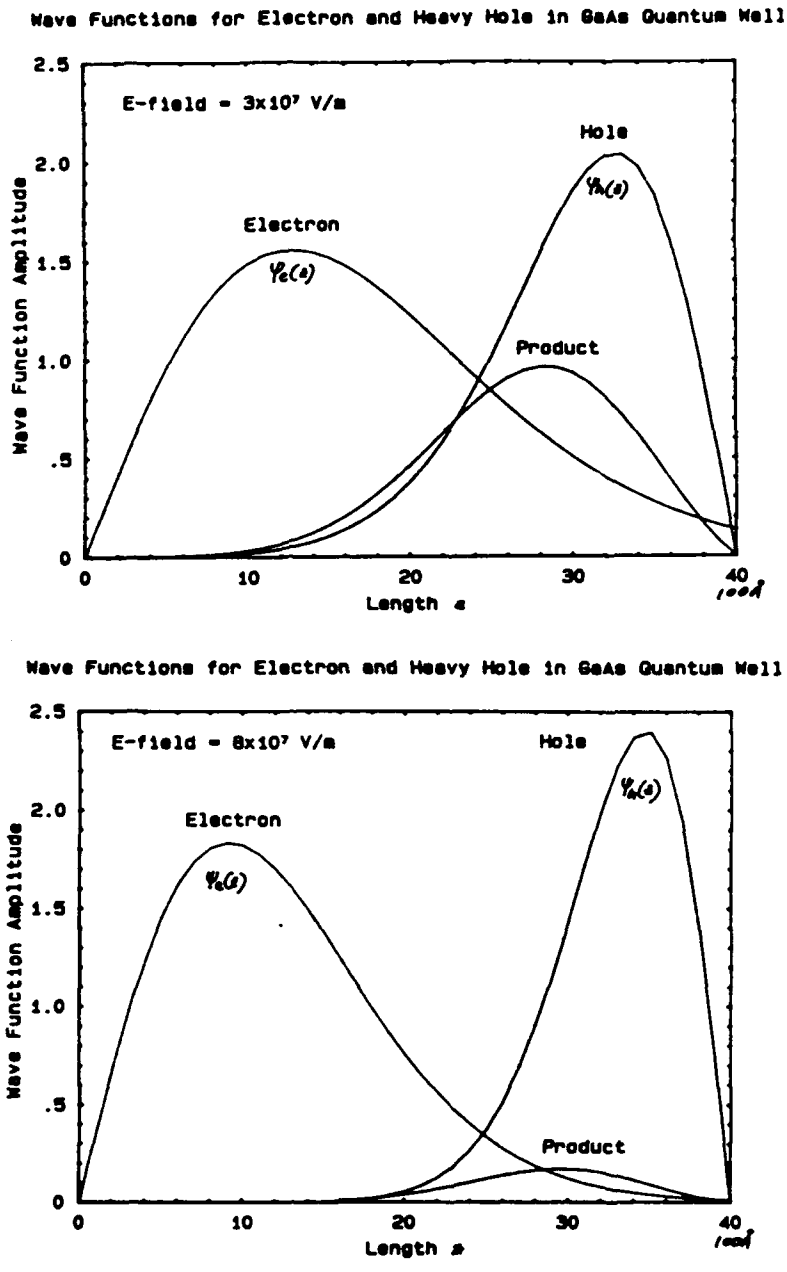

Figure E2. Normalized electron and hole wave functions and their product for fields of a) $3x10^7$ and, b) $8x10^7$ V/m.

Figure E3 shows graphically The change in the overlap integral with increasing E-field. The computations were done for two different well thicknesses, 50 and 100 angstroms. For each case there is a definite range of E-field values where the rate of change is greatest. The curve for the 100 angstrom well also shows where the infinite well approximations cause errors. At zero E-field the curve should approach unity. The computations assume a low lying energy level in a deep triangular potential well. At low E-field levels this is no longer the case and the Airy function solutions cannot be used. However, we can approximate the low field overlap integral values as shown by the dashed line in the figure.

Computing the real and imaginary parts of the refractive index over a wavelength range near the fundamental absorption edge gives the results plotted in figure F4. Note the shift in the peak to lower energies (longer wavelength) as the E-field is increased due to the changing relative energy levels of the electron and hole, and the decrease in amplitude due to the decreasing overlap integral with increasing field.

The energy shift is due partly to a geometric effect. As the potential well tilts more and more with increasing E-field the electron stays toward the bottom

of its well and the hole stays near the top of its well with the net result that the electron and hole are brought closer together, lowering the transition energy. The rest of the energy shift is due to the changing eigenvalues of the particle energies as the shape of the potential well changes.

Figure E5 shows plots of computed absorption coefficient and refractive index variation resulting from the computed complex dielectric constant. From the plots it can be seen that for a given application a wavelength can be chosen that gives maximal change in absorption and a minimal change in refractive index or just the opposite. These computations are in agreement with published experimental data (for example reference 12).

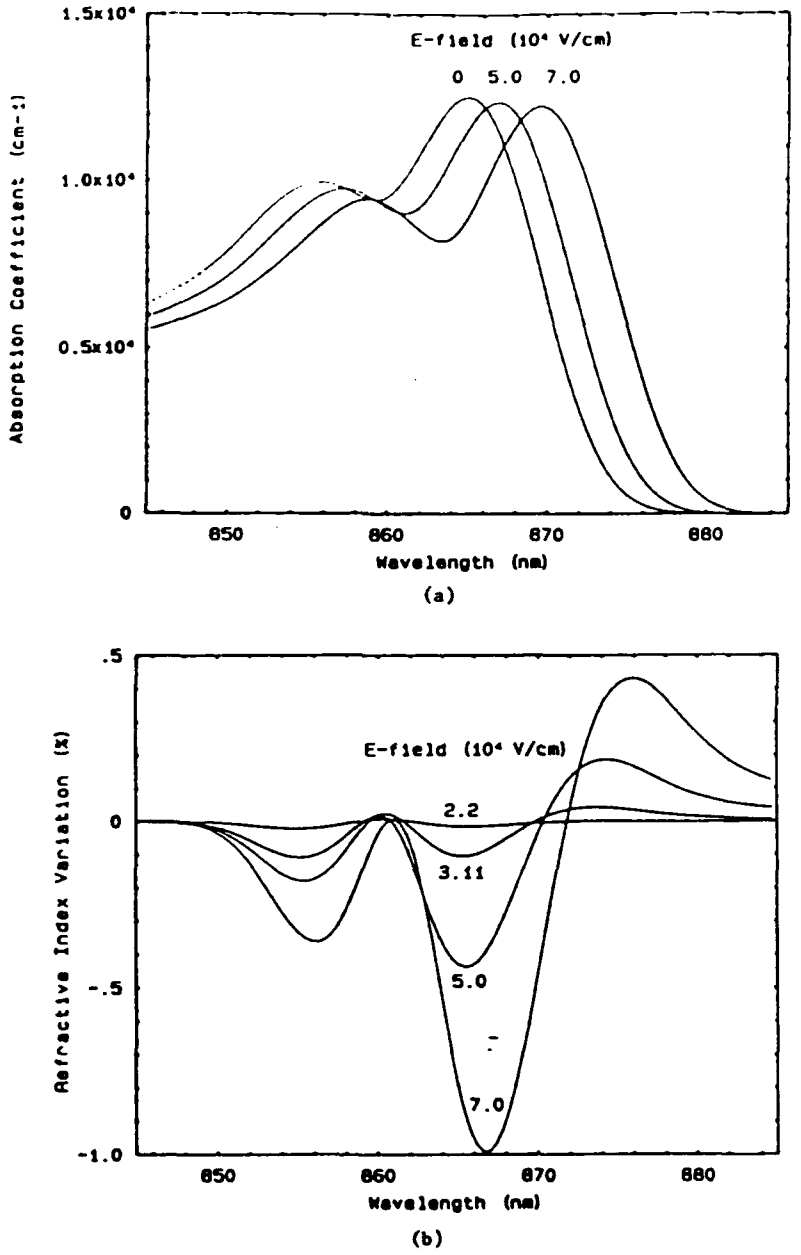

Figure E5. The absorption coefficient (a), and the percent change in refractive index (b), of an AlGaAs quantum well with various E-fields applied.

F. Conclusions

The change in optical properties of semiconductor quantum wells with application of electric field is a highly non linear effect which will have many uses in new integrated optic devices. The ability to predict the optical properties of a wide variety of quantum well materials and geometries is essential.

The results shown in the previous section make clear the fact that the changes in optical properties are sufficient even with moderate electric fields applied to be useful in device applications.

There are many possible ways to generate the electric field that is placed across the quantum wells. Metalized electrodes and doped semiconductor layers around the quantum wells are direct ways to generate a field. Other ways include packets of charge moving through a semiconductor or electron hole pairs formed by optical absorption in surrounding semiconductor layers.

It can be seen that the choice of operating wavelength is critical. If a non-dispersive modulator is being designed the wavelength must be chosen with care and the E-field changes held within limits to keep the refractive index change minimal.

Computations of this type are, therefore, necessary to the design of semiconductor quantum well optic devices.

Appendix 1. Derivations

The following is a more complete derivation of the wave functions and energy levels for bound states in a triangular potential well with infinite barriers [13].

A general form of the time dependent, three dimensional Schroedinger equation is

$$\left(- \frac{\hbar^2}{2m} \nabla^2 + V(\vec{r}) \right) \psi(\vec{r},t) = ih \dot{\psi}(r,t) \ . \quad (1)$$

Since we are involved with quantum well calculations in which the excitons exist in a quasi two dimensional state we will reduce equation 1 to two dimensions, giving,

$$\left(- \frac{\hbar^2}{2m} \frac{\partial^2}{\partial x^2} + V(x) \right) \psi(x,t) = ih \dot{\psi}(x,t) \ . \quad (2)$$

This equation is separable in time, t, giving,

$$\left(- \frac{\hbar^2}{2m} \frac{\partial^2}{\partial x^2} + V(x) \right) \psi(x) = \epsilon \ \psi(x) \ . \quad (3)$$

The potential will be described as shown in figure D1, a triangular potential well with a constant slope and infinitely high potential barriers at x=0 and at x=L. In the region 0<x<L the potential V(x) = ax giving,

$$- \frac{\hbar^2}{2m} \frac{\partial^2 \psi}{\partial x^2} + (ax - \epsilon) \psi = 0 \ ,$$

or,

$$\frac{\partial^2 \psi}{\partial x^2} - \frac{2ma}{\hbar^2}\left(x - \frac{\epsilon}{a}\right)\psi = 0 . \qquad (4)$$

The Airy function solutions can be used if equation 4 can be written in the form of,

$$\frac{d^2\psi}{dw^2} - w\psi = 0 . \qquad (5)$$

This can be done by letting

$$w = \left(\frac{2ma}{\hbar^2}\right)^{1/3}\left(x - \frac{\epsilon}{a}\right) . \qquad (6)$$

Rabinovitch and Zak write this as,

$$w = \alpha_1^{1/3} x - \tilde{\epsilon}\,\alpha_1^{-2/3} \quad , \quad \text{with} \quad \alpha_1 = \frac{2ma}{\hbar^2} ,$$

and $\tilde{\epsilon} = \dfrac{2m\epsilon}{\hbar^2}$.

Using the Airy functions A_i, B_i, gives have the solution (requiring normalization),

$$\psi(x) = \alpha A_i(w) + \beta B_i(w) \quad . \qquad (7)$$

Given the boundary conditions $\psi(0) = \psi(L) = 0$, the equation for the eigenvalues of the energy becomes,

$$A_i(0)\ B_i(L) = A_i(L)\ B_i(0) \quad . \qquad (8)$$

This becomes,

$$A_i(-\alpha_1^{-2/3}\tilde{\epsilon})\ B_i(\alpha_1^{1/3}L - \alpha_1^{-2/3}\tilde{\epsilon}) = B_i(-\alpha_1^{-2/3}\tilde{\epsilon})\ A_i(\alpha_1^{1/3}L - \alpha_1^{-2/3}\tilde{\epsilon}) \quad . \qquad (9)$$

Equation 9 can be solved numerically, but for cases where the wave function energies are small compared to the height of the triangular well, such as when a large electric field is applied, the method can be simplified by neglecting $\tilde{\epsilon}\alpha_1^{-2/3}$ with respect to $\alpha_1^{1/3}L$ and assuming $\alpha^{1/3}L >> 1$. This reduces equation 9 to

$$A_i(-\alpha_1^{-2/3}\tilde{\epsilon})B_i(\alpha_1^{1/3}L) = B_i(-\alpha_1^{-2/3}\tilde{\epsilon})A_i(\alpha_1^{1/3}L) \quad . \qquad (10)$$

Re-writing this as

$$\frac{B_i(\alpha_1^{1/3}L)}{A_i(\alpha_1^{1/3}L)}\ A_i(-\alpha_1^{-2/3}\tilde{\epsilon}) = B_i(-\alpha_1^{-2/3}\tilde{\epsilon})$$

and using the asymptotic form of the Airy functions [14] for the first term reduces this to,

$$2\ \exp[4/3\,\alpha_1^{1/2}\ L^{3/2}]\ A_i(-\alpha_1^{-2/3}\ \tilde{\epsilon}\ ) = B_i(-\alpha^{-2/3}\ \tilde{\epsilon}\ ). \qquad (11)$$

Since, for the conditions mentioned above, the exponential term becomes much larger than the oscillatory Bi term, the expression becomes approximately,

$$A_i(-\alpha_1^{-2/3}\ \tilde{\epsilon}\ ) = 0\ . \qquad (12)$$

So, for the low lying energy levels, which may be of greater interest anyway because they have more effect on the fundamental absorption edge, finding the eigenvalue energy levels becomes a matter of consulting a table of zeros for the Airy function. For example, for the n=1 energy state the first zero of Ai is used (page 478 Ref. 14) giving,

$$-\alpha_1^{-2/3}\,\tilde{\epsilon}\ = -2.3381\ .$$

By substituting in the slope of the well and the width of the well the eigenvalue energy can be calculated.

To get the eigenfunctions, which are the wave functions that are needed for the overlap integral, it is necessary to go back to equation 7 and substitute in the values for w at the boundary x = L which gives,

$$\psi(L) = 0 = \alpha\ A_i(\ Wx=L\ ) + \beta\ B_i(\ Wx=L)$$

or,

$$\alpha A_i(\alpha_1^{1/3} L - \tilde{\epsilon}/\alpha_1^{2/3}) + \beta B_i(\alpha_1^{1/3} L - \tilde{\epsilon}/\alpha_1^{2/3}) = 0 .$$

(13)

Here again the low lying levels in a large E-field approximation is used to reduce this to,

$$\alpha A_i(\alpha_1^{1/3} L) + \beta B_i(\alpha_1^{1/3} L) = 0.$$

Now the asymptotic forms of the Airy function are used again to find that,

$$\frac{\beta}{\alpha} = -1/2 \exp[-4/3 (\alpha_1^{1/3} L)^{3/2}] , \quad (14)$$

which gives for the eigenfunction, up to a normalization constant,

$$\psi_{n(x)} = A_i(\alpha_1^{1/3} x - \tilde{\epsilon}_n/\alpha_1^{2/3})$$
$$- 1/2 \exp[-4/3 (\alpha_1^{1/3} L)^{3/2}] B_i(\alpha_1^{1/3} x - \tilde{\epsilon}_n/\alpha_1^{2/3}) \quad (15)$$

This is the expression used to calculate the electron, light hole, and heavy hole wave functions which are then normalized and the overlap integral computed.

As mentioned before, the wave functions derived above are for an infinite well approximation. These are adjusted to the geometry of interest by using a well width that is larger than the actual quantum well width of the material.

Appendix 2. 'C' code for calculation of Airy Function values.

```
#include <math.h>
#define C1 .35502805
#define C2 .25881940
#define real double

real ftrl(n)
int  n;
{
     real l = 1;
     int  i;
     for (i = 1; i < (n+1); i++)
          l = l * (real)i;
     return (l);
}
airy(z, Ai, Bi)
real z;
real *Ai, *Bi;
{
     real numf, numg;
     real fz, gz;
     int  k;
     fz = 0; gz = 0;
     numf = 1; numg = 1;
     for (k = 0; k < 30; k++) {
          if (k != 0) {
               numf = numf * (real)(3*k-2);
               numg = numg * (real)(3*k-1);
               fz=fz+numf*pow(z,(3*k))/ftrl(3*k);
               gz=gz+numg*pow(z,(3*k+1))/ftrl(3*k+1);
          } else {
               fz = 1;
               gz = z;
          }
     }
     *Ai = C1 * fz - C2 * gz;
     *Bi = sqrt(3.0) * (C1 * fz + C2 * gz);
}
main()
{
     int  i;
     real z, Ai, Bi;
     printf("\n     z     Ai(z)     Bi(z)\n");
     for (i = 0; i < 20; i++) {
          z = (real)i / 2.0*(-1);
          airy(z, &Ai, &Bi);
          printf("\n%f  %f  %f", z, Ai, Bi);
     }
     printf("\n");
}
```

References:

1. R. Dingle, W. Wiegmann, and C. H. Henry, "Quantum States of Confined Carriers in Very THin AlxGa1-xAs-GaAs-AlxGa1-xAs Heterostructures," *Phys. Rev. Lett.*, vol. 33, pp. 827-830, 1974.

2. A. Zehe, et al., "Resonant Tunneling Through a Double Barrier Single V-Shaped Quantum Well", *Superlattices and Microstructures*, Vol. 7, No. 1, 1990.

3. T. Ishikawa, et al., "Quantum-Confined Stark Effect in a Parabolic-Potential Quantum Well", *Japanese Journal of Applied Physics*, Vol. 29, No. 8, 1990.

4. K. Betterchargee, F. Jain, G. Drake, OSA Topical conference on Spatial Light Modulators, September 1990.

5. R. Dingle (Editor), *Semiconductors and Semimetals, Vol. 24, Applications of Multiquantum Wells, Selective Doping, and Superlattices*, Academic Press Inc., New York, 1990.

6. A. K. Gahtak, I. C. Goyal, R. L. Gallawa, " Mean Lifetime Calculations of Quantum Well Structures: A Rigorous Analysis", *IEEE J. Quantum Electronics*, Vol.

26, No. 2, February 1990.

7. D. Miller, et al., "Band-Edge Electroabsorption in Quantum Well Structures: The Quantum Confined Stark Effect", *Physical Review Letters*, Vol. 53, No. 22, 1984.

8. D. A. B. Miller et al., "Electric Field Dependence of Optical Absorption Near the Band Gap of Quantum-Well Structures," *Phys. Rev. B*, vol. 32, pp. 1043-1060, 1985.

9. *J. Wilson, J. F. B. Hawkes, Optoelectronics, An Introduction*, Prentice/Hall International, New Jersey, 1983.

10. R. Hunsperger, *Integrated Optics: Theory and Technology*, 2nd Ed., Springer-Verlag, New York, 1985.

11. J. Dimmock, "Introduction to the Theory of Exciton States in Semiconductors", in *Semiconductors and Semimetals Vol.3* (R. Dingle ed.). p.259, Academic Press Inc., New York, 1979.

12. Y. Kan et al., "Field Effects on the Refractive Index and Absorption Coefficient in AlGaAs Quantum Well

Structures and Their Feasibility for Electrooptic Device Applications", *IEEE J. of Quantum Electronics*, vol. QE-23, pp. 2167-2180, 1987.

13. A. Rabinovitch, J. Zak, "Electrons in Crystals in a Finite-Range Electric Field," *Phys. Rev. B*, vol. 4, pp. 2358-2370, 1971.

14. *Handbook of Mathematical Functions*, M. Abramowitz, I. Stegun Ed., Dover Publications, New York, 1970, equations [10.4.59] and [10.4.63].